CHALMERS

Mathematical modelling and thermodynamic optimization of a CO_2 heat pump cycle

Master of Science Thesis in the Master Degree Programme, Sustainable Energy Systems

Brendan Daley
Oskar Redlund

Department of Energy and Environment
Division of Heat and Power Technology
CHALMERS UNIVERSITY OF TECHNOLOGY
Gothenburg, Sweden, 2012

THESIS FOR THE DEGREE OF MASTER OF SCIENCE

Mathematical modelling and thermodynamic optimization of a CO_2 heat pump cycle

Master of Science Thesis in Sustainable Energy Systems (MPSES)

BRENDAN DALEY, OSKAR REDLUND

SUPERVISORS:
Åsa Jardeby
Roger Nordman

EXAMINER:
Lennart Vamling

CHALMERS

Department of Energy and Environment
Division of Heat and Power Technology
CHALMERS UNIVERSITY OF TECHNOLOGY
Gothenburg, Sweden, 2012

Mathematical modelling and thermodynamic optimization of a CO_2 heat pump cycle

Master's Thesis within the Sustainable Energy Systems programme

BRENDAN DALEY
OSKAR REDLUND

Department of Energy and Environment
Division of Heat and Power Technology
Chalmers University of Technology
SE-412 96 Göteborg
Sweden
Telephone + 46 (0)31-772 1000

Chalmers Reproservice
Göteborg, Sweden 2012

Mathematical modelling and thermodynamic optimization of a CO_2 heat pump cycle

Master's Thesis within the Sustainable Energy Systems programme
BRENDAN DALEY, OSKAR REDLUND
Department of Energy and Environment
Division of Heat and Power Technology
Chalmers University of Technology

Abstract

Due to the harmful environmental effects of HCFC's (hydrochlorofluorocarbons) and CFC's (chlorofluorocarbons) discovered in the late 20th century, interest has increased for more environmentally-friendly refrigerant alternatives in cooling systems. One of the alternatives is carbon dioxide due to its unique properties, low cost, and low environmental impact compared to conventional refrigerants.

The aim of this report is to study the use of CO_2 in a one-stage and two-stage heat pump cycle for transportation purposes using an existing HCFC-based heat pump modified to work with CO_2. Tests were conducted on this existing experimental CO_2 heat pump setup at SP Technical Research Institute of Sweden in Borås, Sweden.

A model was developed with MatLab software primarily for the two-stage compression configuration, and the results of the model were validated against measurements conducted with the experimental setup. Overall, the measurement and model results showed that the gas cooler unit is over-dimensioned and modifications in future systems could be considered. It was found that the air side within each heat exchanger limits the heat transfer in the existing setup due to the ratio of outside to inside surface area and the low air heat transfer coefficient. Measurements results also indicate that there is significant uneven distribution at the entrance to the evaporator unit. This creates uncertainty when modelling as it is too complicated with the existing measurements and equipment to model anything other than perfect distribution at the inlet to the evaporator unit.

Results also indicate that the 2nd stage compressor operates at a much lower efficiency than expected by manufacturer and theoretical data. Tests on compressor operating speed changes showed significant system performance improvements when decreasing the 2nd stage compressor speed from the manufacturer suggested value. It was also found that there are possibilities for improving the system performance such as installing an internal heat exchanger.

Key words: CO_2, heat pump cycle, modelling, refrigerant, two-stage compression, heat transfer

Matematisk modellering och termodynamisk optimering av en CO_2 värmepumpcykel

Examensarbete inom masterprogrammet Sustainable Energy Systems
BRENDAN DALEY, OSKAR REDLUND
Institutionen för Energi och Miljö
Avdelningen för Värmeteknik och maskinlära
Chalmers Tekniska Högskola

1 Sammanfattning

Med anledning av upptäckter under 2000 – talets senare del angående miljöpåverkan från olika HCFC och CFC ämnen har intresset för mer miljövänliga köldmedier för kylsystem ökat. Ett av alternativen är koldioxid på grund av ämnets unika egenskaper, låga kostnad samt en mindre miljöpåverkan jämfört med konventionella köldmedier.

Syftet med denna rapport är att studera användandet av CO_2 i en befintlig ett- och två-stegs värmepumpcykel vilken är designad för en HCFC inom transportsektorn. Cykeln har modifierats för att kunna användas med CO_2 som köldmedia. Tester har utförts på den befintliga experimentella värmepumpcykeln lokaliserad vid SP Sveriges Tekniska Forskningsinstitut i Borås, Sverige.

En modell av den befintliga värmepumpscykeln har utvecklats primärt för två-stegs kompression och resultaten som modellen ger har validerats mot mätresultat utförda på värmepumpcykeln. Allmänna resultat visar på att gaskylaren är överdimensionerad, vilket betyder att modifieringar kan övervägas vid design av framtida system. Det konstaterades också att luftsidan inom värmeväxlarna var den begränsande sidan gällande det totala värmeutbytet. Detta beror på förhållandet mellan ut- och insidornas area samt den låga värmeöverföringskapaciteten för luft. Resultat från mätdata indikerar också på en väldigt ojämn distribution vid inloppet till förångaren. Denna ojämna distribution skapar osäkerhet i modellen och dess resultat eftersom allt annat än jämn distribution är för komplicerat att modellera med tillgängliga mätmetoder och mätinstrument.

Resultat indikerar också på att kompressorn som används för andra stegets kompression opererar med mycket lägre effektivitet än vad som förväntas utifrån både teoretiska värden och de värden som tillverkaren fastställt. Tester med ändrat varvtal för andra stegets kompressor till lägre varvtal visar på att en mycket högre effektivitet kan uppnås jämfört med tillverkarens föreslagna värden. Det konstaterades också att det finns andra möjligheter till effektivisering av systemets prestanda, ett exempel är att installera en intern värmeväxlare.

Nyckelord: värmepumpcykel, modellering, köldmedia, två stegs kompression, värmeväxling

Table of Contents

Acknowledgments

We would first like to thank our examiner Lennart Vamling for giving up his valuable time to help us and for his continued advice throughout the project. Lennart has provided great support that made it possible to complete this report.

We would also like to thank our supervisor Åsa Jardeby for her help at SP in conducting experiments, taking the time to answer our questions about the test rig, and providing us with a basic literature list and advice to start our studies.

We would also like to thank Roger Nordman and Lennart Rolfsman for interesting discussions and advice regarding our work at SP.

Finally, we would like to thank Patrik Ollas, Gael Seené, Amir Shabanzadeh and Marmar Ghorbani for the good company and maintaining a nice atmosphere in our office room.

1 Background

1.1 History of CO_2 as a refrigerant

Carbon dioxide was one of five main refrigerants dominating the markets in the late 19th century along with ether, ammonia, sulphur dioxide and methyl chloride. The main factors influencing the refrigerant choice for new systems were the ease of use, reliability, safety, space required, efficiency, and installation cost. All of the main refrigeration systems used were to some extent hazardous due to either very high operating pressures (in the case of CO_2), toxicity, or flammability. Carbon dioxide became the dominant refrigerant in the marine industry in the late 19th and early 20th centuries despite higher system construction costs. It was much cheaper than alternative refrigerants, required very low coal consumption to drive the system, and was more reliable than the open-circuit air systems used at that time. For land systems, ammonia dominated the markets because ammonia plants for chilling or freezing were cheaper and could be run more efficiently. Ammonia based systems were further developed in the early 20th century and soon became more feasible than carbon dioxide systems due to improved safety and technology, even for marine systems.

As the 20th century progressed, carbon dioxide was phased out in favour of other refrigerant systems as shown in Figure 1 below.

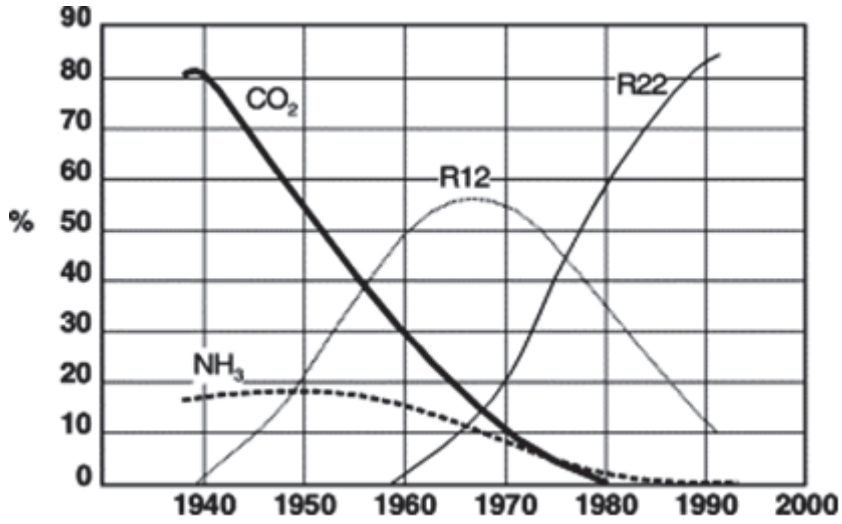

Figure 1. Usage rates of main refrigerants in existing marine systems (Kim M. P., 2004).

1.2 Resurgence of CO_2 as a major refrigerant

As the world population grows and standard of living increases in poorer countries, the demand for efficient and cost-effective heating and cooling devices will probably remain high. However, concerns have arisen in the last several decades about the environmental costs of using some popular refrigerants for these devices, such as HCFC's and CFC's. Many of these artificial refrigerants have been found to be powerful greenhouse gases which potentially lead to environmental problems when leaked or improperly disposed of.

The discussion about exactly what the consequences will be from emitting excess amounts of greenhouse gases is a controversial topic, especially in modern politics. Despite these political issues,

the leaders of most countries in the world were able to come to an agreement about the potential dangers of some refrigerants, ratifying the Montreal Protocol as part of the United Nations Vienna Convention for the Protection of the Ozone Layer, organized in the 1980's and 1990's. The Montreal Protocol mandates the phasing out of CFC's and HCFC's, among other harmful chemicals, due to their effect on ozone. Specifically, the Montreal Protocol mandates a gradual elimination of CFC and HCFC production in all ratifying member states, with zero production of refrigerants used in new technologies by 1 January 2010 (Montreal Protocol, 2000).

The phasing out of some common CFC and HCFC refrigerants such as R-12 and R-22 due to these regulations has led to research on possible replacements, including refrigerant mixtures and natural refrigerants such as CO_2. One group of replacement alternatives as mentioned by Nekså was HFC's (hydrofluorocarbons) (Nekså P. , 2002). However, HFC's have a high environmental impact as well due to their high global warming potential (GWP). They are therefore included in the Kyoto agreement as compounds that should be regulated, and are no longer considered as viable alternatives to reduce greenhouse gas emitting refrigerants.

CO_2 is commonly considered to have a low environmental impact and a net environmental impact of zero when it is used from the waste products of industrial or energy production. CO_2 is also non-toxic, non-flammable, cheap, and readily available. Gustav Lorentzen is commonly referred to as the first person to reinvestigate the use of CO_2 as a refrigerant, developing a prototype in 1989 due to a belief in the potential advantages of CO_2 systems partly because of the refrigerant's positive characteristics. Lorentzen and Petterson published in 1992 results of tests on their prototype for automobile applications, showing similar cycle coefficient of performance (COP) for CO_2-based systems compared to conventional refrigerants despite non-ideal test conditions for their CO_2 system. The results showed that CO_2 could potentially compete with conventional refrigerants, sparking an increased interest for CO_2-based systems (Kim M. P., 2004). Due to this research and the improved technology to limit safety concerns from high pressures, research on CO_2 as a viable refrigerant has increased considerably in recent years (Pearson, 2005).

2 Project aim

This project aims to study and suggest improvements for an existing vapour-compression cycle heat pump prototype with CO_2 as the working fluid. This experimental heat pump setup is located at SP Technical Research Institute of Sweden in Borås, Sweden. This master thesis project is part of a larger project at SP on heat pump research. The driving force behind the overall project is that EU directives are expected to come in the near future limiting the use of harmful refrigerants in commercial transport devices. Existing EU directives on refrigerant use affect personal vehicles but not large transport vehicles. Due to these expected regulations, SP has decided to modify an existing commercial heat pump using an HCFC as a working fluid into the current CO_2-based setup. To decrease costs and time consumption related to testing the technical feasibility of this heat pump prototype, this master thesis project was started to develop a mathematical computer model of the experimental test setup using MatLab software.

The model should be capable of predicting system behaviour for various settings such as expansion valve outlet conditions, system mass flow, outside air conditions, and amount of superheat. The model should be capable of operating with either one-stage or two-stage compression to respectively simulate cold air ($T_{\mathrm{air}} \approx 0°\mathrm{C}$) and freezing air ($T_{\mathrm{air}} \approx -20°\mathrm{C}$) evaporator outlet scenarios. Upon completion of the model, the model was used to suggest optimum operating conditions of the test setup for various operating modes and to suggest design changes to the test setup for further optimization of the COP. It is also important to note that the although suggestions will be made for further optimization of the experimental setup, the existing setup is built primarily for testing purposes rather than to be an optimal final design.

There are difficulties involved in modelling a system used for transportation purposes. The system runs on outside air, with properties that can vary significantly depending on the day, time of year, and location. Therefore, the model needs to be able to handle a rather wide span of operating points.

3 Overview of the system

Figure 2 shows a simplified sketch of the test setup. The main purpose of the setup is to maintain cooled air for refrigeration systems. The setup can be run in a two-stage compression "freezing" mode for desired air temperatures around -20℃, or a one-stage compression "cooling" mode for desired air temperatures around 0℃. In one-stage compression mode, the high pressure 2nd stage compressor and intermediate cooler are bypassed. The refrigerant then flows from point 2 into the gas cooler instead of through the points 2, 3 and 4 into the gas cooler, as seen in Figure 2 below. For two-stage compression mode, the CO_2 is cooled between the two compressors. The desired operating temperature of the CO_2 into the evaporator for one-stage compression mode is around -10℃, and for two-stage compression mode below -25℃. These temperatures are achieved by expanding the CO_2 after the gas cooler to a certain pressure that corresponds to a temperature for a given enthalpy.

The most important purposes of the evaporator are to both cool down the air to the desired temperature and at the same time ensure that the CO_2 is fully evaporated before entering the 1st stage low pressure compressor. Eventual CO_2 liquid that is not fully evaporated in the evaporator is stored in the liquid separator tank shown in Figure 2 below. The associated liquid release valve can be opened to release eventual liquid that becomes trapped in the separator tank. As discussed later in this report, the gas cooler outlet temperature is very important and related to the system COP. It is therefore important to cool the CO_2 as much as possible in the gas cooler since lower temperature CO_2 has a higher enthalpy for a given pressure than higher temperature CO_2. The intermediate cooler is crucial to avoid overheating the 2nd stage compressor. Despite the intermediate cooler, the 2nd compressor overheats when there are high ambient air temperatures. Therefore, in the model developed, a simple internal heat exchanger has been added and can be enabled for high ambient temperatures to avoid over heating of the 2nd stage compressor. The internal heat exchanger is not illustrated in Figure 2, but this heat exchanging takes place between point 7 and 3 in the model.

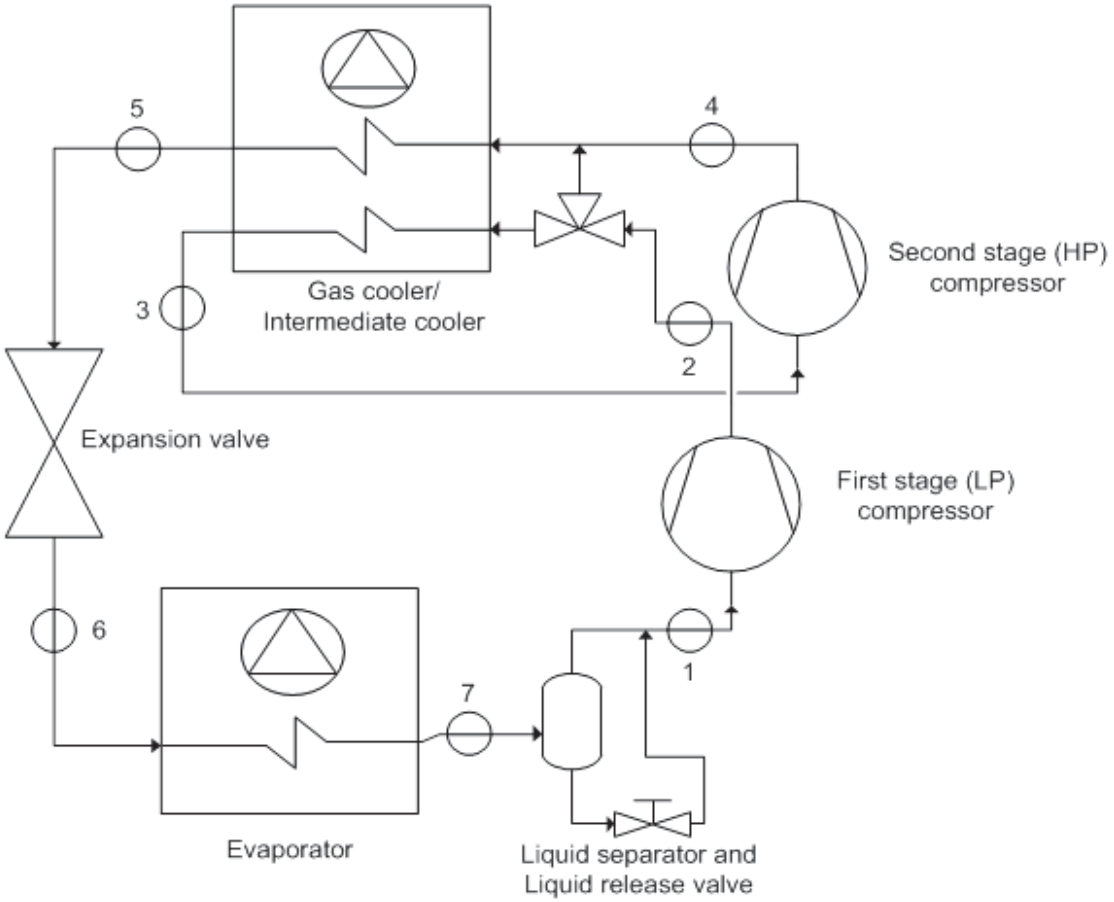

Figure 2. Simplified system diagram featuring the main components; modified from Jardeby et. al (2012).

4 Experimental methodology

This section provides a brief description of the test setup used to obtain the measurement data, and the basic motivation for the test procedure used.

4.1 Experimental setup

The existing experimental setup was originally designed for experimentation purposes at SP Technical Research Institute. A device was used to measure electrical signals from the experimental setup. These were then sent to a computer for data logging and conversion of the electrical signals to useful values according to earlier calibration tests.

A brine system was used to regulate the air inlet temperatures to the heat exchangers to ensure more accurate test results and to be able to simulate different ambient air conditions. The brine system is a system of tubes with a salt water solution that pass through each of the heat exchanger units, maintaining the air temperature with minimal losses. The brine system tubes are also well insulated outside of the main components to further minimize losses.

Well-insulated thermocouples had been attached to the outside of tubes and outside of all the main components of the system for temperature measurements of the CO_2 at the entrance and exit of each component. Six thermocouples had also been added to both the gas cooler and evaporator units to measure air temperature. The thermocouples were placed a short distance in front and after the tubing at the air entrance and exit and spread evenly along the entire length of the heat exchanger. These were used to test for uneven air distribution at the entrance to the heat exchangers. Since previous tests had shown the temperature differences to be minimal between the thermocouples for each heat exchanger, the tests conducted for this report used only the middle thermocouples in each heat exchanger for air temperature measurements. Minor modifications were made to the existing measurement setup to test for uneven refrigerant distribution around the evaporator expansion device. For these modifications the now unused air thermocouples were placed on the tubes near the inlet to the evaporator to be able to measure the temperatures before and after the distributor more accurately. Pressure sensors had also been installed to measure the refrigerant pressure at the inlet and outlet to each of the main components. These pressure sensors were kept in place for the measurements conducted by the authors of this report.

It was also desired to measure air and CO_2 temperature differences inside the gas cooler and intercooler heat exchanger unit. However, it is too difficult to place any thermocouples on the tubes inside the heat exchanger units due to the small space between the tubes and the closely spaced fins. This is also the reason why for the thermocouples attached to the evaporator tubing it was only possible to place thermocouples on the tube bends outside of the main exchanger area. Therefore, the measurements within the gas cooler and intercooler are from the pre-existing air temperature thermocouples and the inlet and outlet refrigerant thermocouples. In the model, the air flow generated by the fans is therefore assumed to be well-mixed and is divided between the gas cooler and the intermediate cooler with respective to their sizes.

4.2 Motivation for testing

In order to develop a more accurate model, tests were conducted on the experimental setup to study typical system performance. Tests were performed during several different days at varying system conditions. During each test, the heat pump system was allowed to reach steady-state operation for several minutes to obtain more accurate measurement data for typical system performance. These tests were then used to measure the accuracy of the initial model predictions, such as refrigerant mass flow rate and component outlet temperatures and pressures.

It was initially desired to add into the model predictions for the performance of the 2nd stage compressor based upon the inlet and outlet pressures of the 1st stage compressor. An initial idea for testing this was to test the system effect of directly changing the 1st stage compressor inlet and outlet values, but this is not possible with the experimental setup. The only way to change the compressor pressures while maintaining the same mass in the system was to manually change the expansion valve outlet pressure setting. Tests were also conducted to measure the system changes with changing evaporator superheat, but it proved too difficult to measure and maintain a constant superheat. Therefore, for the purposes of this report, the expansion valve outlet pressure was chosen as one of the major independent variables during testing.

Additional tests were conducted after analysis of the first several days of testing since it was observed that the 2nd stage compressor performed poorly in comparison to the manufacturer predictions. These additional tests included reducing the operational speed of the second stage compressor to observe a possible increase in system performance. The results of these tests will be presented later in the Results section of this report.

5 Properties of CO_2

To provide a better understanding of the use of CO_2 as a refrigerant, some of the unique properties of CO_2 are presented here.

Carbon dioxide has a low critical temperature of 31.1°C compared to other typical refrigerants. Due to the properties of CO_2, typical vapour compression cycles with CO_2 as the refrigerant often operate at pressures near or above the critical pressure of 73.8 bar during the heat rejection process. Such cycles are referred to as transcritical due to the operation of the cycle at both subcritical and supercritical pressures (Kim M. P., 2004).

The properties of CO_2 vary widely as the temperature approaches the pseudo-critical temperature T_{pc}, the temperature where the specific heat of CO_2 is highest. As seen in Figure 3 below, thermal conductivity, k, dynamic viscosity, μ, and density, ρ, increase exponentially near T_{pc} for decreasing temperature. With decreasing pressure, μ and ρ both decrease slightly at the pseudo-critical temperature, whereas k increases slightly. One of the most interesting aspects is the rapid change in c_{p} around T_{pc}, resulting in underestimation of the heat transfer coefficient using traditional heat transfer modelling equations (Lemmon, 2010).

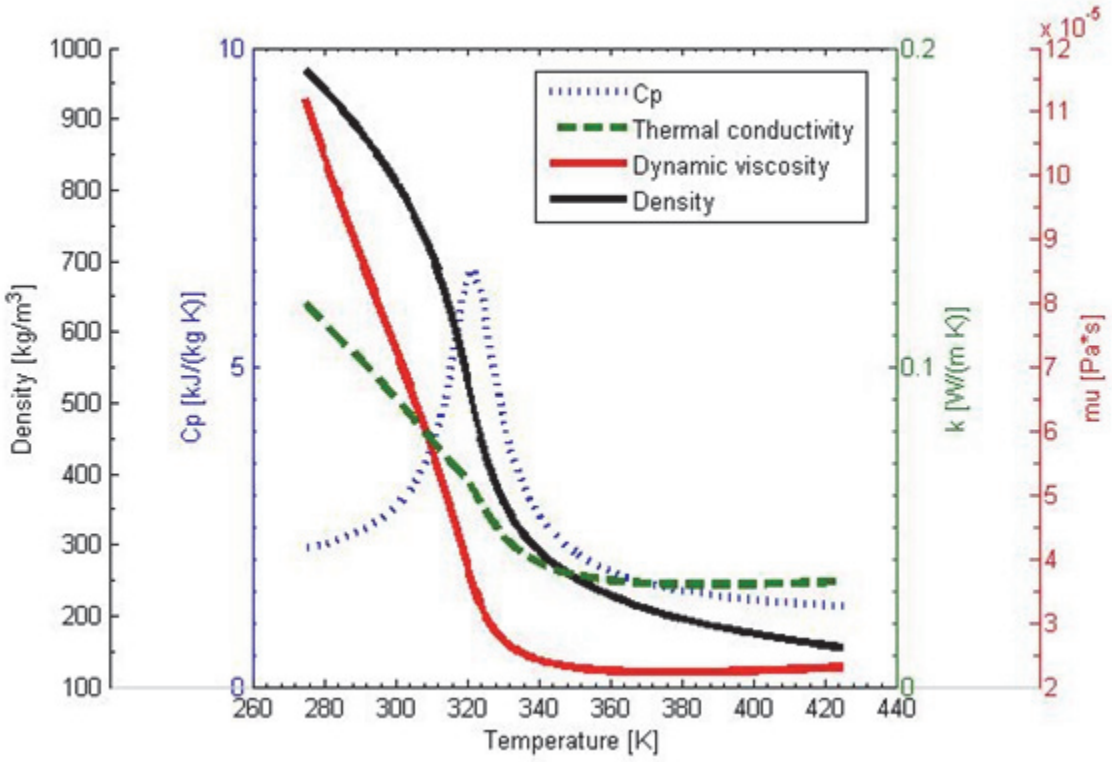

Figure 3. Thermo-physical property changes of CO_2 near $\mathbf{T_{pc}}$ at 10.7 MPa.

As shown in Figure 4 - Figure 7 below, the specific properties vary widely in a relatively low temperature span around the pseudo-critical temperature.

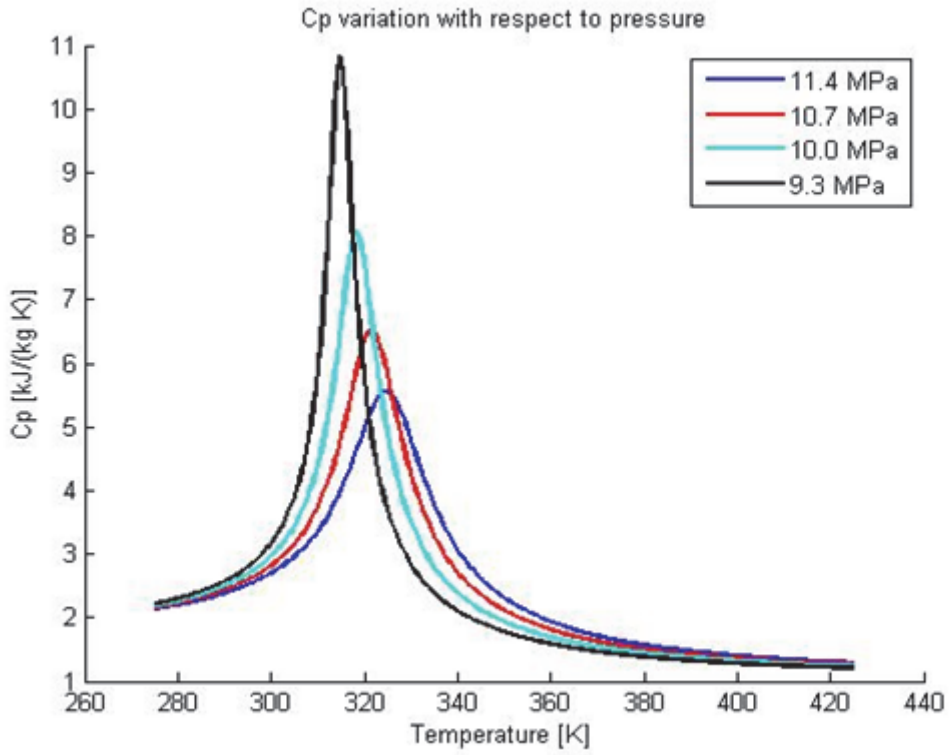

Figure 4. Large $\mathbf{c_p}$ variation of CO_2 near $\mathbf{T_{pc}}$ for expected 2nd-stage compressor outlet pressures.

This effect is even more pronounced for pressures around the critical pressure of 73.8 bar, as seen in Figure 5 below. As the pressure gets very close to the critical pressure, c_p becomes infinitely high.

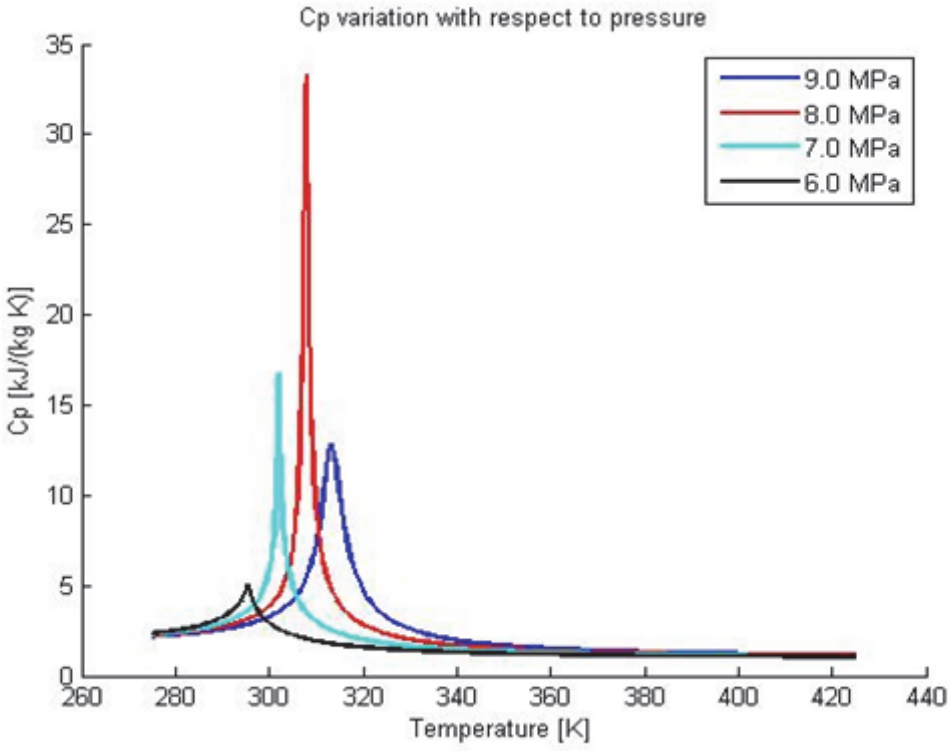

Figure 5. Large $\mathbf{c_p}$ variation of CO_2 near $\mathbf{T_{pc}}$ for expected one-stage compressor outlet pressures.

Below follows examples of how the density varies at different pressures.

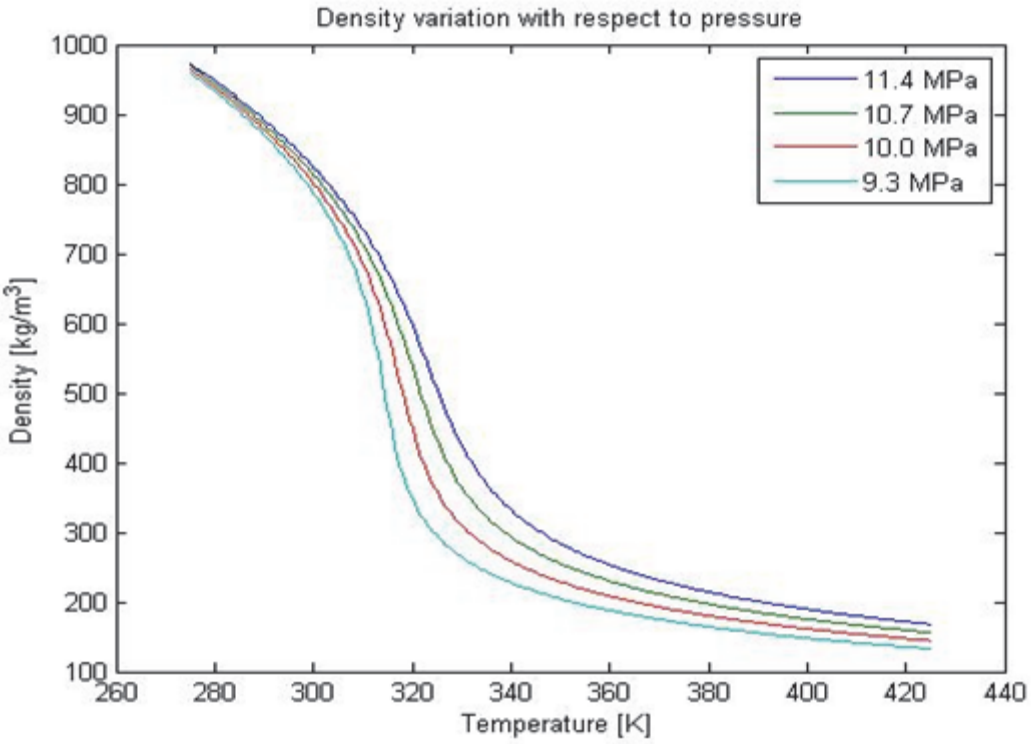

Figure 6. Density variation of CO_2 near $\mathbf{T_{pc}}$ for expected 2nd-stage compressor outlet pressures.

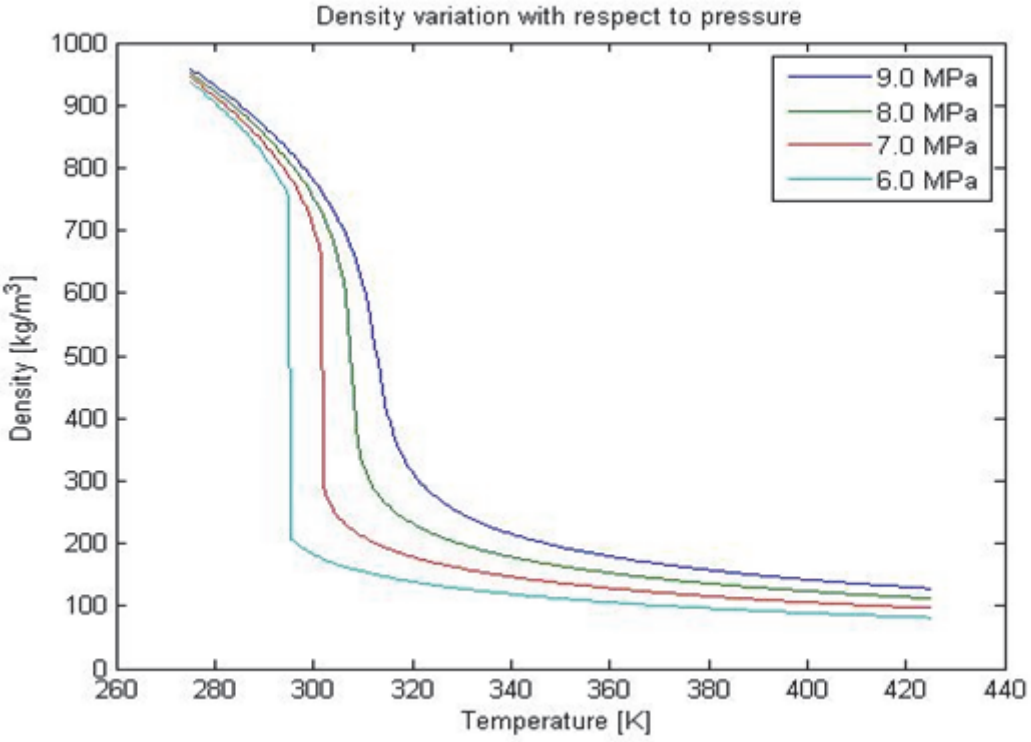

Figure 7. Density variation of CO_2 near $\mathbf{T_{pc}}$ for expected one-stage compressor outlet pressures.

6 Literature review

To understand the current expert knowledge with regard to CO_2 heat pump cycles, an extensive literature review was conducted. Below follows the results of this literature review, with a focus on CO_2 heat pumps specifically but with mention of other vapour-refrigeration heat pump cycles when no specific information for CO_2 was found.

One important point to first note is the size of the tubing used for the existing experimental setup that was studied for this report. The tubing ranged in size from about 7 mm to 10 mm inside diameter. There is no standard for the specification of macro and micro-scale tubing, though a literature review by Thome et. al (2005) suggested the use of inside diameters smaller than 3 mm for micro-scale and diameters larger than 3 mm for macro-scale (Thome J.R., 2005). It is important to consider the assumptions for macro and micro scale used since for a constant diameter tube the flow characteristics, including heat transfer coefficients and pressure drops, can change significantly depending on the testing conditions (Thome J.R., 2005). The correlations for macro-scale tubing were used for this report after literature review showing consistent use of macro-scale assumption with diameters larger than 5 mm for similar conditions of CO_2 flow.

6.1 Pressure behaviour

Park et. al (2007) studied heat transfer and pressure drop for various refrigerants in two-phase flow in a horizontal smooth tube of 6.1 mm inside diameter (Park C. H., 2007). The results showed increased CO_2 pressure drop for decreased saturation temperature, increasing quality, and increased mass flux. Similar results were observed by Park et. al (2007) for both R410A and R22, as seen in Figure 8 below. For saturation temperature of -30°C, the highest observed pressure drop for CO_2 by the authors was about 10 kPa/m at a mass flux of 400 kg/(m^2s) and about 2 kPa/m at a mass flux of 200 kg/(m^2s). At equivalent mass fluxes and saturation temperatures, the measured pressure drop of CO_2 in the Park et. al (2007) studies was much lower than that of R410A and R22. The pressure drop of CO_2 was much less because CO_2 has lower vapour velocities due to its higher vapour density. Also, the pressure drop for all the refrigerants increases when the evaporation temperature is reduced due to a reduction in vapour density and an increase of liquid viscosity. The tests by Park et. al (2007) also showed that the Müller-Steinhagen and Heck correlation can predict the measured pressure drop for CO_2 rather well, and that the Friedel correlation was able to predict the measured pressure loss data with low error.

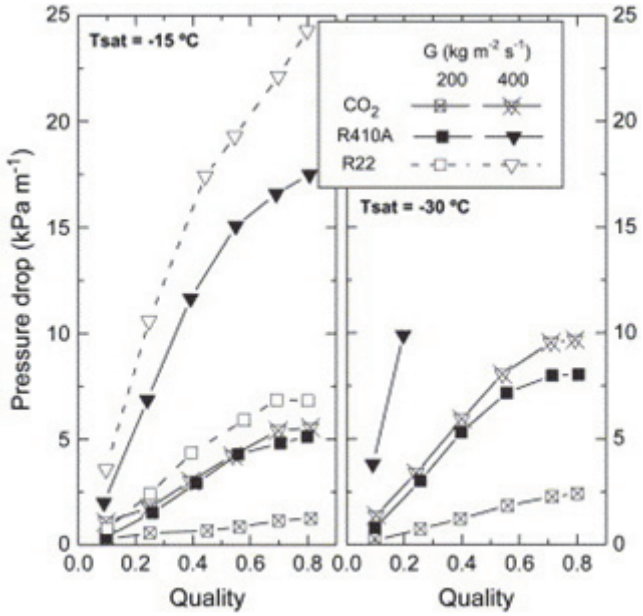

Figure 8. Pressure drop of adiabatic two-phase flow for CO_2, R410A and R22 with the change of mass flux and quality at the evaporation temperatures of -15 and -30℃ (Park C. H., 2007).

Yoon et. al (2003) studied heat transfer and pressure drop for CO_2 in a gas cooler with horizontal copper tubes of 7.73 mm inside diameter (S. H. Yoon et. al, 2003). Data was measured for CO_2 inlet pressure between 7.5 and 8.8 MPa, and for varying mass fluxes. The observed pressure drop for all tests was less than 1 kPa/m, only a small percentage of the CO_2 inlet pressure. Pressure drop was observed to decrease as the CO_2 inlet pressure increased due to the density of carbon dioxide increasing with increased system pressure. Similar to the tests carried out by (Park C. H., 2007) described above, in the tests conducted by Yoon et al. the pressure drop also increased with an increase in mass flux in the gas cooler.

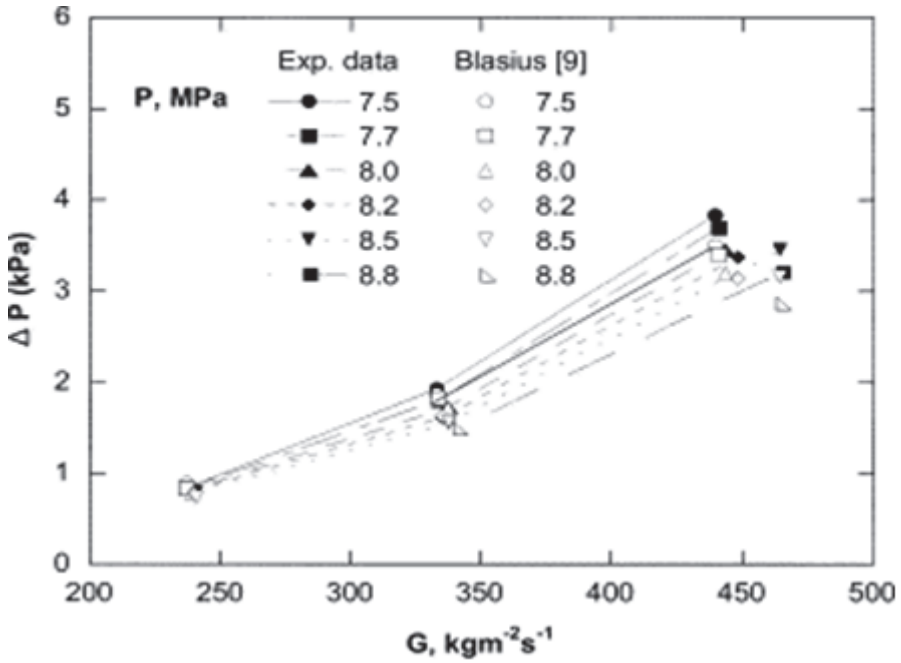

Figure 9. Measured and computed pressure drop in a gas cooler at different mass fluxes and inlet pressures (S. H. Yoon et. al, 2003).

In the tests by Yoon et. al (2003) the pressure drop also increases at a higher rate relative to the mass flux at lower pressures, as shown in Figure 9. The results also showed very good agreement between the measured and predicted pressure drops calculated with the Blasius equation, the most common correlation used for pressure drop in smooth tubes for turbulent flow. Yoon et. al (2003) found the flow in the supercritical region to be somewhat similar to single phase flow and therefore the authors suggest that the Blasius correlation is reasonable to use to predict pressure drop of supercritical CO_2 in a gas cooler.

6.2 Gas cooler heat transfer

As described in the CO_2 properties section, the characteristics of CO_2 differ significantly depending on the current state of the fluid. Son et. al (2006) studied CO_2 heat transfer and pressure drop in a horizontal tube gas cooler with inside diameter of 7.75 mm (Son, 2006). Tests were measured for supercritical CO_2 at the inlet of the gas cooler for mass fluxes between 200 and 400 kg/(m^2s). Similar to the studies mentioned above, the authors measured pressure drop was in good agreement with the predictions from the Blasius correlation.

Son et. al (2006) showed that the measured local heat transfer coefficient for a certain pressure varies heavily depending on the current temperature for a constant mass flux. For the early stages of cooling, the variation of the heat transfer coefficient was very small due to the high temperatures of the CO_2 where the properties only vary a small amount. In the tests performed by Son et. al (2006), when CO_2 temperatures approached the pseudo-critical temperature, the heat transfer coefficient varied rapidly with even small temperature changes. The authors compared measured results for heat transfer coefficient to those predicted by the Bringer-Smith correlation and found good agreement for temperatures far from the pseudo-critical point but large error near the pseudo-critical point due to high c_p in the measured CO_2 flow. The authors developed a new correlation for heat transfer in supercritical CO_2 gas coolers and were able to predict the majority of the measured data within 18%.

Son et. al (2006) also discussed that the heat transfer coefficient changes very rapidly with change in temperature for given pressures, as seen in Figure 10 below. From Figure 10 it can also be noted that the heat transfer coefficient only changes marginally with higher temperatures and more rapidly closer to the critical temperature region as discussed above. Another important note here is that the inlet pressure only has a minor effect on the variation of the thermodynamic properties over a wide temperature span. The CO_2 properties vary only slightly with different pressures at high temperatures in early cooling stages and at lower temperatures than the critical temperature in later cooling stages.

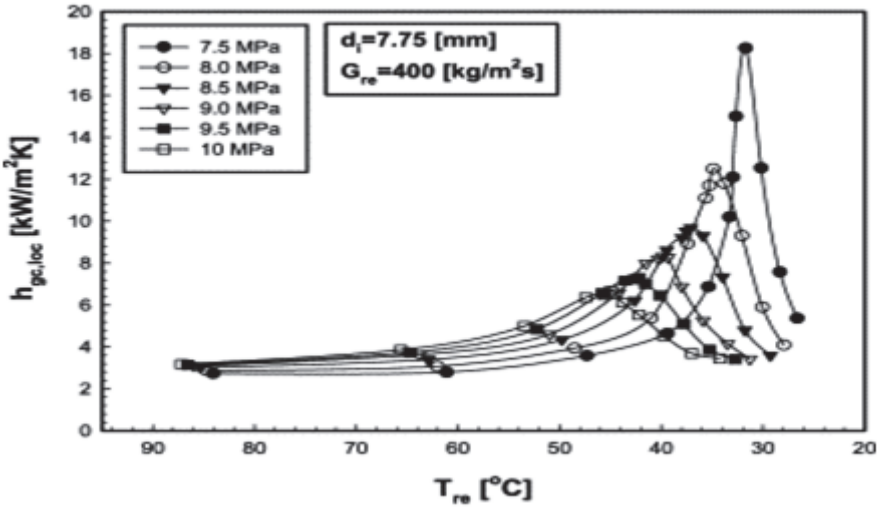

Figure 10. Heat transfer coefficient for a constant mass flux for different pressures in a gas cooler (Son, 2006)

J. Pettersen et. al (1998) also points out that the heat transfer coefficient in supercritical gas cooling is heavily affected by the temperature and pressure of the CO_2 for single phase flow (J. Pettersen et al., 1998). In the near-critical region, the properties of CO_2 show irregularities which affect the heat transfer coefficient. Those irregularities cause the standard correlations to predict unrealistic values at those conditions. Therefore, correlations developed for property variations are needed to estimate realistic numbers in those regions (J. Pettersen et al., 1998).

However, the heat transfer coefficient also varies with different mass fluxes for a given pressure. For all pressures tested in a paper from Yoon et. al (2003) the heat transfer coefficients increased due to the increase in Reynolds number (S. H. Yoon et. al, 2003). The authors found that for high CO_2 temperatures, the mass flux affected the heat transfer coefficient only to a small degree. Meanwhile the heat transfer coefficient was greatly affected by the mass flux in lower CO_2 temperature regions near the critical temperature. The peak value of the heat transfer coefficient was also found to increase when the mass flux is increased.

6.3 Evaporator heat transfer

Several studies investigated CO_2 boiling heat transfer coefficients at evaporation temperatures lower than 0°C. Bredesen et al. (1997) studied boiling heat transfer for CO_2 evaporation at -25, -10, and 5°C in 7.0 inner diameter smooth tubes, Høgaard et al. (1997) for CO_2 evaporation at -25 and -10°C in 10.06 mm diameter tubes, and Park et al. (2005) for CO_2 evaporation at -30 and -15°C in a 6.1 mm inner diameter tube (Bredesen, 1997); (Høgaard, 1997); (Park C. e., 2005). All three studies determined that the nucleate boiling heat transfer coefficient is a more important factor in the total heat transfer coefficient for CO_2 than for other refrigerants (Park C. H., 2007).

Park et al. (2007) showed that the heat transfer coefficient is almost independent of the vapour quality of CO_2 compared to a large increase of the heat transfer coefficient for R410A and R22 with increasing vapour quality. When comparing the heat transfer coefficient relative to the mass flux, it was seen that for R410A and R22 at this evaporation temperature the heat transfer coefficient

increases quite rapidly as the mass flux increases. For high qualities there was a smaller observed increase in heat transfer coefficient for CO_2 for increased mass flux, and an unexpected decrease in heat transfer coefficient for low qualities (Park C. H., 2007). A similar decrease in heat transfer coefficient was also observed at low qualities by Bredesen et al. (1997).

The heat transfer coefficient was observed by Park et al. (2007) to have a more positive slope at higher mass fluxes for all refrigerants because the convective heat transfer coefficient becomes larger with higher mass fluxes and therefore contributes more with higher quality. Figure 11 below shows the comparison discussed above that shows the heat transfer coefficient for the three different refrigerants at different mass fluxes with constant heat flux and saturation temperature (Park C. H., 2007).

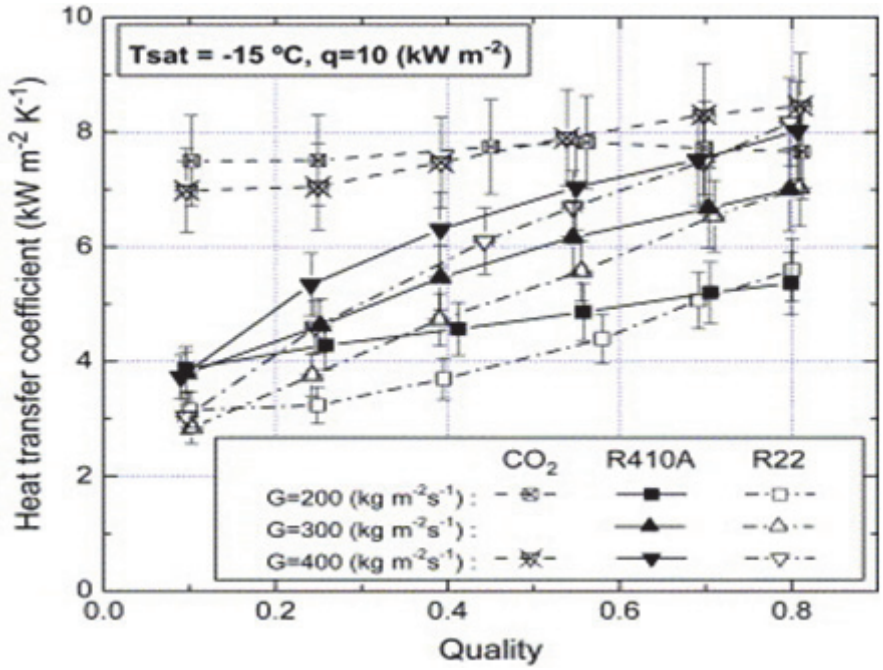

Figure 11. Heat transfer coefficient comparison for CO_2, R410A and R22 with respect to mass fluxes and quality at the evaporation temperature of -15℃ and the heat flux of 10 kW/m^2 (Park C. H., 2007).

The difference in heat transfer coefficients between CO_2 and the other mentioned refrigerants was explained by a larger pool boiling heat transfer contribution for CO_2 than the others. That is also why the gap between the heat transfer rates for each refrigerant was bigger at lower qualities where the pool boiling dominates compared to the convective boiling. The convective boiling contribution to the total boiling heat transfer coefficient was similar for all investigated refrigerants for a known quality (Park C. H., 2007).

Yun et. al (2003) studied heat transfer coefficients for CO_2 and R134A boiling in horizontal 6 mm inside diameter tubes at varying mass flux and saturation temperatures of 5 and 10℃. The authors observed a decreasing CO_2 heat transfer coefficient as quality increased, the opposite effect of that commonly measured for typical refrigerants such as R134A, R410A, and R22. For the case of increased evaporation temperature from 5 to 10℃, heat transfer coefficients were even higher at low qualities and even lower at the high qualities. The left side graph of Figure 12 below shows the results from the study and the right side graph show results from a study made by Cho et al. (2000).

For a temperature increase from -25 to -10℃ the heat transfer coefficient increased for all vapour qualities (Cho, 2000); (Yun et. al, 2003).

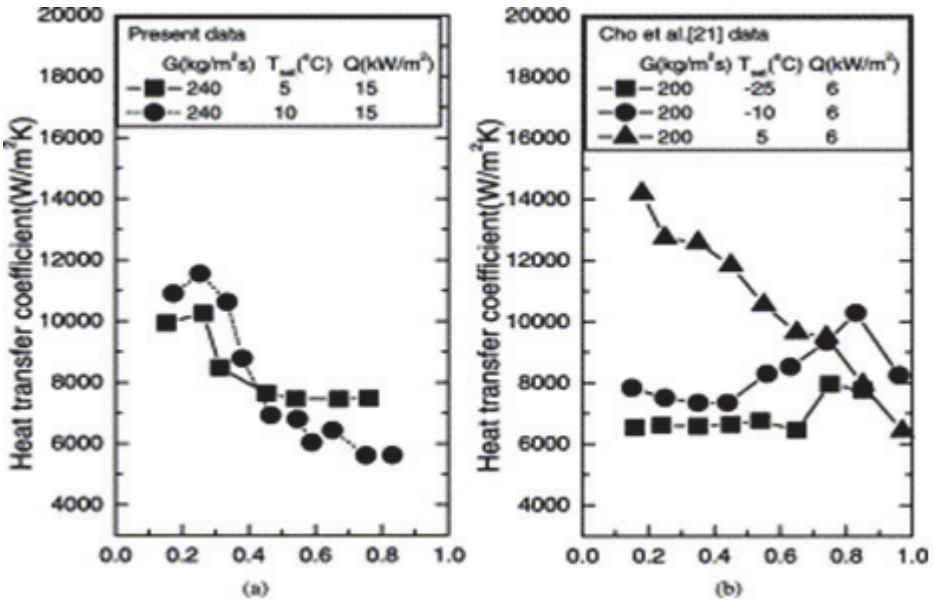

Figure 12. (Yun et. al, 2003).

The decrease in heat transfer coefficient for increasing quality for CO_2 was explained due to the dominance of nucleate boiling at lower qualities for CO_2 and by partial dryout of the CO_2 liquid film occurring at lower qualities than for typical refrigerants. The much lower surface tension of CO_2 and lower liquid film flow rate compared to typical refrigerants is responsible for the increased dryout of CO_2 in the unstable annular flow regions at low qualities (Yun et. al, 2003).

Similar conclusions found by Park (2007) described above are also presented by Yun et. al (2003) concerning mass flux and heat transfer coefficients. In the study by Yun et. al (2003), for vapour qualities between 0.2 and 0.5, the heat transfer coefficient only depends marginally on the mass flux since the nucleate boiling dominates that region. For higher vapour qualities, 0.5 to 0.8, Yun et. al (2003) observed a heat transfer coefficient increase with increased mass flux due to the more notable addition of convection.

Park (2007) also explains that the nucleate boiling heat transfer is reduced with decreasing evaporation temperature, which is explained by the temperature and pressure relations. This explains the results presented by Yun et. al (2003) where the heat transfer was really high for low qualities and high evaporation temperatures and rapidly decreased when the quality increased and the nucleate boiling became less dominant.

Due to the unique two-phase flow and thermophysical properties of CO_2, predictive methods for boiling heat transfer coefficients are very complicated. Existing correlations developed for other refrigerants commonly under predict the boiling heat transfer coefficients for two-phase CO_2 flow. Several experimental studies have been conducted to develop updated correlations for two-phase CO_2 flow, notably the Cheng et. al (2008) correlation and the Yoon et al. (2004) correlation. These studies were conducted for various tube diameters, mass fluxes, and evaporating temperatures (Mastrullo et. al, 2010).

Mastrullo et. al (2010) compared heat transfer coefficient data from previous literature studies and new measured data for two-phase CO_2 flow to coefficients predicted by common correlations developed for both CO_2 and other refrigerants. The experimental setup of Mastrullo et. al (2010) consisted of pure CO_2 operating under different conditions in smooth horizontal circular tubes with inner diameter of 6 mm. This study was performed to compare the accuracy of the most common boiling heat transfer coefficient correlations depending on different common evaporator operating conditions. The results are shown in Figure 13 below and it can be seen that the predicted heat transfer coefficient varies significantly depending on correlation used (Mastrullo et. al, 2010).

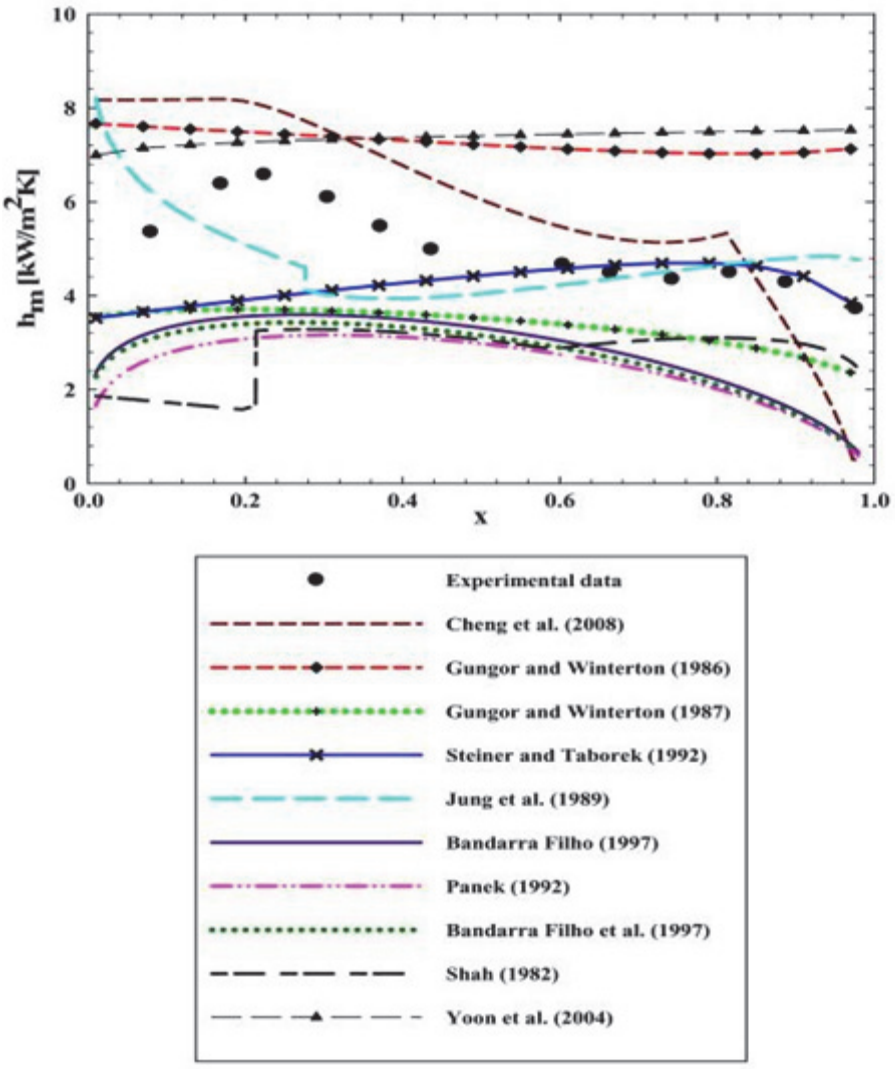

Figure 13. Direct comparison of the experimental heat transfer coefficients against predicted values for G = 201 kg/(m^2s), T_{sat} = 4.2°C and q = 9.6 kW/m^2 (Mastrullo et. al, 2010).

It can be noted that none of the correlations could predict the measured heat transfer coefficients well for the various two-phase flow qualities. The Cheng et. al (2008) correlation, which was developed specifically for CO_2 followed the experimental trend for qualities between 0.2 and 0.8 but beyond 0.8 predicted significant heat transfer decrease which was not observed in the experimental results . The Yoon et al. (2004) correlation was also developed specifically for CO_2 but over predicted the heat transfer significantly and predicted mostly constant heat transfer coefficients for all qualities (Mastrullo et. al, 2010).

For this specific case studied by Mastrullo et al. (2010), the Jung et al. (1989) method developed as a general correlation for flow boiling had the lowest mean error of 21.6%; only able to predict about 75% of the data within 30% error (Mastrullo et. al, 2010). This level of error seems to be common in the literature, as most previous studies demonstrate that existing correlations do not work well to predict the flow boiling heat transfer coefficients of CO_2 (B. T. Austin, 2011).

6.4 Distributor

The design of distributors is today based on empirical data since there is no general way of predicting the distribution of two-phase flow. The distribution depends on many factors such as operating conditions, fluid properties, and channel geometry which makes it very difficult (Marchitto, 2008). Most studies concerning flow distribution study common refrigerants or fluids. However, as CO_2 has only recently been rediscovered as a refrigerant, there are few studies researching flow distribution issues with CO_2 as the refrigerant. Therefore, the descriptions here are presented as more of a summary of what can be expected in the experimental setup, though more research may be needed for CO_2 specifically.

Many studies have been performed to investigate flow distribution of two-phase flow from headers into multiple tubes at either the top or bottom of a heat exchanger unit. Non-uniform distribution is common and it is very difficult to achieve a uniform distribution. Gravity separation of the two fluid phases also increases the problem for horizontal headers. Earlier research and patent literature suggests two ways of improving the distribution. The first method is to adjust the tube projection of the header or install obstacles such as throttle plates at the inlet of the header. Local feeders into the tubes are also an option, which requires special distribution devices. Small distributor diameter has been proven to reduce the distribution problems. Although, special designs are only viable for a given operating condition and when the operating conditions are altered, the design must be changed to maintain proper distribution (Webb, 2005).

As one example, Ahmad et al. (2009) studied two-phase distribution of HFE 7100 around 100 kPa and 57℃ for vertical and horizontal tubes with varying header geometries. The authors found significant flow maldistribution which was heavily influenced by the header diameter, fluid mass flow rate, inlet fluid quality, and the vertical or horizontal set-up condition (Ahmad, 2009).

Brix et al. (2009) developed a 1-D steady state numerical simulation model for two-phase flow distribution in an evaporator for R134A with two parallel microchannel tubes. As distribution became more uneven mass flow rate decreased, especially in the channel with higher vapour inlet quality, leading to incomplete evaporation in the second channel in some cases and therefore reduced cycle efficiency (Brix, 2009). This is in agreement with the results from literature studies that indicate flow maldistribution has an important effect on cycle performance (Vist S. , 2004).

In previous studies, Vist and Pettersen studied two-phase refrigerant distribution of R134A in 10 parallel round tubes. The results showed major distribution differences within the tube configuration. In both vertical and horizontal tests, the vapour phase was much more likely to flow within the tubes closest to the inlet whereas the opposite effect was seen with the liquid refrigerant (Vist S. P., 2002) and (Vist S. P., 2003). Further tests for tube diameter differences with CO_2 and R134A as the refrigerants indicated somewhat better distribution for tubes with 8 mm inner diameters compared to those with inner diameter of 16 mm, but too much liquid was still observed in the final two farthest tubes in both tests (Vist S. , 2004).

6.5 Advantages and issues

The most remarkable property of CO_2 is its low critical temperature of 31.1℃. Operation close to the critical temperature gives CO_2 refrigerant systems important features (Nekså P. , 2002).

Carbon dioxide based refrigeration systems compete very well with systems using other refrigerants with respect to energy efficiency when sub critical operation is possible (Nekså P. , 2002). Sub critical operation is however only possible for refrigeration systems when the average heat sink temperature is rather low. The COP in sub critical operation is limited by the highest heat sink temperature. When the heat sink temperature is high, heat is rejected at supercritical pressure. This means that the cycle is transcritical and operates partly above and below the critical pressure. In transcritical operation, the COP is mostly limited by how low refrigerant temperature it is possible to achieve after the heat rejection takes place. This means that the lowest heat sink temperature sets the limitation.

Compared to HFC refrigerant systems, CO_2 systems seem to be more efficient at lower ambient temperatures and perform worse at warmer ambient temperatures (Nekså P. e., 2010). Therefore, when comparing the efficiency of CO_2 systems with alternative systems it is important to consider the operating conditions the systems will experience. A system will most likely only experience operating conditions close to the design point during parts of the year, so a comparison should include variable operating conditions apart from optimal operating conditions.

High operating pressures are a concern in CO_2-based heat pump operation where pressures can be about 5-10 times those in systems using other common refrigerants. This problem is no longer an impediment to increased use of CO_2 heat pumps as modern manufacturing is able to supply the necessary components to safely operate at these pressures (Sarkar, 2006). In particular, CO_2 compressors need thicker walls to contain high operating pressures (Kim M. e., 2004). One potential concern with the high operating pressures is related to flying materials or other shock effects in case of a burst tube. However, Nekså et. al (2010) explains that the explosion energy for CO_2 heat pump systems is similar to that of other common refrigerants due to the smaller tube diameters typically used for CO_2 systems. This is in agreement to measurements by Pettersen for comparison of CO_2 and R22 explosion energy (Pettersen, 1999); (Kim M. e., 2004).

CO_2 has a very high volumetric capacity compared to common alternatives; up to 5-10 times higher. Therefore, despite high pressures compact compressors are possible. Two advantages of this is that the overall compressor size can be much smaller than that needed for other refrigerants (Kim M. e., 2004); (Nekså P. , 2002) and CO_2 compressors have the ability to operate at speeds of 3000 rpm. The high volumetric capacity, in combination with very good heat transfer characteristics, enables use of compact heat exchanger units compared to common refrigerants and thereby reduces system costs.

CO_2 compressors are only affected by a small amount of valve pressure drops, which leads to small re-expansion losses and thereby higher efficiencies. This is because of the higher operating pressure level and the different shape of the pressure-volume diagram (Nekså P. , 2002). Losses due to internal leakage around the piston and valves are shown to be very small for CO_2 compressors - less than 1% - and therefore negligible for a properly designed reciprocating compressor (Kim M. e., 2004).

Despite the classification of CO_2 as non-toxic and its use in many products such as beverages, prolonged exposure to certain levels of CO_2 in air can have moderate to severe effects on human

health. Moderate effects such as headaches and increased breathing rate can be observed at concentrations of around 2% by volume in air. Although 10% by volume is the lowest reported concentration that is lethal to humans, severe effects can occur at concentrations above 4% and this is therefore the Immediate Danger to Life and Health concentration suggested by the US government workplace safety regulations (Kim M. e., 2004).

6.6 Optimization

The outlet temperature of the gas cooler in a trans-critical CO_2 system is very important and closely related to the system COP since the enthalpy changes rapidly with a change in temperature for high pressure CO_2. Therefore, gas coolers for CO_2 systems are designed to cool the CO_2 as close to the air inlet temperature as possible. CO_2 systems exit gas cooler temperature affects the COP more than the exit temperatures for other refrigerant systems. Other ways of reducing the temperature after the gas cooler could be for example to have an internal heat exchanger in the system as long as it doesn't overload other parts of the cycle (J. Pettersen et al., 1998). Sarkar (2006) also mentions that it has been demonstrated that internal heat exchange has the potential to increase the cycle efficiency by up to 25% (Sarkar, 2006). This is because the irreversibility at the throttle is relatively high in a basic transcritical CO_2 cycle.

Many CO_2 cycles use heat exchangers with flow distributed over multiple microchannel tubes due to the high system pressures (Sarkar, 2006) and for heat exchanger efficiency reasons (Kim M. e., 2004). In particular, the use of flat microchannel tubes can significantly increase refrigerant-side surface area and decrease the air-side pressure losses. Microchannel heat exchangers can increase system costs but have been used where compact heat exchangers are desired (Sarkar, 2006). However, since the temperatures vary quite rapidly in especially CO_2 gas coolers, internal conduction between fins, tubes, and manifolds may cause performance reduction. Possible solutions to internal conduction include splitting fins, dividing heat exchangers into sections, and proper manifold geometry design (Sarkar, 2006).

In a recent publication from Sarkar (2010), the use of an ejector-expansion device to modify the system performance of a CO_2 is discussed. In such a system, the liquid and vapour is separated before the evaporator and the vapour cycles back through the compressor and gas cooler while the liquid passes through the evaporator. This type of ejector-expansion could significantly improve the COP of a cycle and simplify the gas cooler pressure control. Results from previous experiments show that an ejector-expansion device can improve the system COP compared to a conventional CO_2 cycle to a similar degree as an internal heat exchanger addition described above. However, the ejector-expansion device needs to be carefully designed and many parameters will influence the overall performance of the cycle (Sarkar, 2010).

There has been a lot of research concerning modifying the cycle performance of CO_2 cycles. Examples are internal heat exchanging, ejection expansion device, work recovery expansion machine and compressor economization. Studies referenced by Sarkar (2010) show that the biggest COP improvements are achieved by the most costly modifications even if lower cost modifications also may lead to significant improvements (Sarkar, 2010). A more detailed investigation of these modification techniques are beyond the scope of this report, however, studies show that major improvements are indeed possible regarding transcritical CO_2 compression cycles.

7 Model methodology

In this section the theoretical basis for the computer model is described in detail. A brief discussion on the main modelling assumptions is included, as well as a detailed description of the equations used to simulate each of the main components in the heat pump cycle.

7.1 General model assumptions

The model developed for the test setup includes some basic overall assumptions in addition to the assumptions made for the different components as presented later in the Model methodology section. Expansion of CO_2 within the expansion valve is assumed to be isenthalpic, the system is considered to have no CO_2 leakage to the surroundings, and there is no fouling for CO_2 inside the tubes. The oil leakage from the compressors is considered negligible since the lubricating oil is soluble with the CO_2 and oil levels within the compressors remained the same after many months of testing. For the air side, the air pressure drop throughout the heat transfer units is assumed to be negligible. The inlet air temperature into the gas cooler and intercooler is assumed to be a set value depending on the outside air conditions simulated, meaning that the outlet temperature simulated remains constant over time. Heat transfer between the CO_2 and ambient air for the tubing outside the main system components is considered negligible due to the very low heat transfer coefficient of natural convection. Additionally, the constants used in the model for thermal conductivity of the aluminium fins and copper tubing are 237 and 401 W/(m.K), respectively.

The thermocouples installed on the tubes in the experimental setup measure the wall temperature of the tube, not the bulk temperature of the CO_2. This causes problems when the actual CO_2 temperature is needed to determine the enthalpy before the expansion valve and just before the compressors. Since the bulk temperature cannot be measured accurately, it is assumed to be the same as the wall temperature. This leads to a possible error source if the bulk temperature differs significantly from the wall temperature. Assuming that the bulk temperature and the wall temperature are the same causes however no modelling problems. Estimated pressure drop values were used to calculate the wall temperatures after the distributors. These values were obtained using REFPROP and assuming isenthalpic expansion. This method was used because it was shown to be more accurate to predict the pressure drop rather than the temperature change over the distributors.

7.2 Air side

To calculate the heat transfer from the air side in the intercooler, gas cooler and evaporator, the air properties must first be determined. In the experimental test setup at SP, air moves in cross flow over the tubes in what is assumed for the model to be a staggered configuration as seen in Figure 14 below.

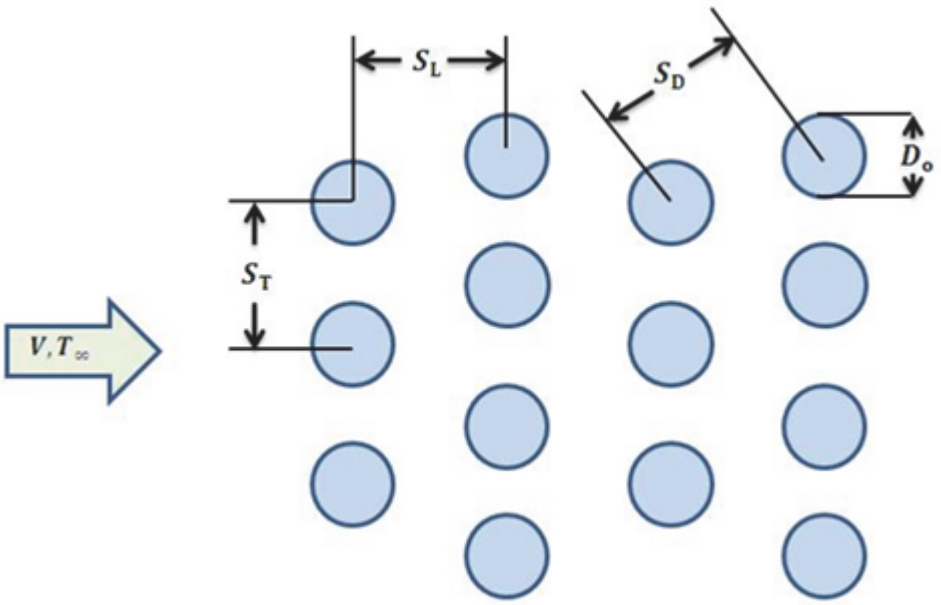

Figure 14. Example of a cross flow tube bank configuration, adapted from (F.P. Incropera et. al, 2007)

The actual tube configurations is as seen in Figure 17 and Figure 18, where S_T, S_L, and S_D are 0.021, 0.0127 and 0.0165 m, respectively, and D_o is the tube outside diameter. To simplify calculations this configuration has been assumed for the model even though in the test setup the tubes are not perfectly staggered as shown. The limitations of this assumption will be further discussed in the Discussion section of this report.

To determine the air properties and heat transfer, the maximum velocity of air in the tube configuration, V_{max}, is calculated by

$$V_{max} = \frac{S_T}{2(S_D - D_o)} V \quad (1)$$

For the case of

$$2(S_D - D_o) < (S_T - D_o)$$

Otherwise,

$$V_{max} = \frac{S_T}{S_T - D_o} V \quad (2)$$

This gives a maximum Reynolds number of the airflow in the tube configuration according to

$$Re_{max} \equiv \frac{\rho V_{max} D_o}{\mu} \quad (3)$$

In order to calculate a heat transfer coefficient for the air, an average Nusselt number in the entire tube configuration is calculated using the correlation from (Zukauskas, 1972), equation (4). This correlation for heat transfer over the entire tube bank is used since the spacing between tubes is very small. For a case with sufficiently spaced tubes, other correlations for single tubes can be used.

$$\overline{Nu} = C_1 C_2 Re_{\max}^{m} Pr^{0.36} \left(\frac{Pr}{Pr_{\mathrm{w}}}\right)^{1/4} \quad (4)$$

In equation (4) the air properties are evaluated at the mean of the fluid inlet and outlet temperature at a constant pressure, except for Pr_{s}. For the experimental test setup studied in this report, Pr_s is assumed to be the same as Pr since the Prandtl number only changes slightly with temperature at atmospheric pressures.

C_2 is a constant dependent on the tube configuration and the number of tube rows, N, for

$$Re_{\max} \gtrsim 1000$$

$$N < 20$$

And C_1 and m are constants given by (Grimison, 1937), which are dependent on the values of

$$\frac{S_{\mathrm{T}}}{D_{\mathrm{o}}} \quad (5)$$

$$\frac{S_{\mathrm{L}}}{D_{\mathrm{o}}} \quad (6)$$

For

$$N < 20$$

$$0.7 \lesssim Pr \lesssim 500$$

$$1000 \lesssim Re_{\max} \lesssim 2 \times 10^6$$

The constants C_1, C_2, and m for the test setup examined are 0.465, 0.569 and 0.95, respectively.

With the average Nusselt number for the tube configuration, the average heat transfer coefficient for the air side is given by

$$h_{\mathrm{air}} = \frac{\overline{Nu} k_{\mathrm{air}}}{D_{\mathrm{o}}} \quad (7)$$

The method used to calculate the heat transfer in each heat exchanger unit will be explained in the respective sections for the different heat exchanger components. However, it is necessary to briefly discuss here the modelling process for determining the temperature difference for the air between tube passes. For modelling purposes, one pass of tubes is considered to be one vertical row as shown in Figure 14 above. The average temperature of the air over the entire pass, T_{air}, is assumed to be constant for the entire length of one pass and all tubes within that pass. The model is an iterative model, where for a starting value the average temperature difference for air from one pass to the next, ΔT_{air}, is used based upon the expected inlet and outlet air conditions for the entire heat exchanger unit. At the end of each pass in the model, the actual temperature difference for air from one pass to the next is calculated by

$$\Delta T_{\mathrm{air}} = \frac{\dot{Q}_{\mathrm{pass}}}{\dot{m} c_{\mathrm{p}}} \quad (8)$$

Where $\dot{Q}_{\mathrm{pass}}$ is the calculated heat transfer for all segments in one pass, calculated in the Gas cooler and Evaporator parts of the Model methodology section. In the next iteration of the model, the updated ΔT_{air} for each pass replaces the old value and the average air temperature used for modelling in each pass is taken as the average of the updated inlet and outlet temperature values for a pass. The model is then iterated until the outlet temperature of the CO_2 from the entire heat exchanger unit converges.

7.2.1 Fins

Between the tubes, fins are installed to increase the heat transfer between the air side and the refrigerant side. The fins are very thin rectangular fins parallel to the air flow with a uniform cross section throughout the length. In total, there are 375 fins in the evaporator and 390 fins in the gas cooler and intermediate cooler. Each fin covers all tubes of the units and has the same depth and length as the unit itself. For modelling purposes, each fin is divided into small sections representing the heat transfer area close to each individual tube so the heat transferred from each small section can be calculated. The fin heat transfer contribution is calculated by the following equation for convective heat transfer for fins of a uniform cross section (F.P. Incropera et. al, 2007)

$$\dot{Q}_{\mathrm{fin}} = M \frac{\sinh(mL) + \left(\frac{h_{\mathrm{air}}}{m k_{\mathrm{fin}}}\right)\cosh(mL)}{\cosh(mL) + \left(\frac{h_{\mathrm{air}}}{m k_{\mathrm{fin}}}\right)\sinh(mL)} \quad (9)$$

Where

$$m = \sqrt{\frac{h_{\mathrm{air}} P}{k_{\mathrm{fin}} A_{\mathrm{c}}}} \quad (10)$$

$$M = \sqrt{h_{\mathrm{air}} P k_{\mathrm{fin}} A_{\mathrm{c}}}\,\theta_{\mathrm{b}} \quad (11)$$

$$\theta_{\mathrm{b}} = T_{\mathrm{b}} - T_{\infty} \quad (12)$$

Where *P* is the perimeter of the fin, A_c is the cross sectional area of the fin, T_{b} is the temperature at the base of the fin, and T_{∞} is the temperature of the ambient air. For each segment in the model T_{b} is approximated by the temperature of CO_2 for the inlet of the segment, and T_{∞} is approximated by the temperature of air in the middle of the pass.

For rectangular fins the cross sectional area and the perimeter are given by

$$A_{\mathrm{c}} = wt \quad (13)$$

$$P = 2w + 2t \quad (14)$$

Fin performance was determined using the following efficiency equations where

Fin efficiency is

$$n_{\mathrm{fin}} \equiv \frac{\dot{Q}_{\mathrm{fin}}}{\dot{Q}_{\mathrm{max}}} = \frac{\dot{Q}_{\mathrm{fin}}}{h_{\mathrm{air}} A_{\mathrm{f}} \theta_{\mathrm{b}}} \quad (15)$$

With the surface area of the fin defined by

$$A_{\mathrm{f}} = 2wL_{\mathrm{c}} \quad (16)$$

Fin effectiveness is a ratio of thermal resistances, which is given by

$$\varepsilon_{\mathrm{f}} = \frac{R_{\mathrm{t,b}}}{R_{\mathrm{t,f}}} = \frac{\dot{Q}_{\mathrm{fin}}}{h_{\mathrm{air}} A_{\mathrm{c}} \theta_{\mathrm{b}}} \quad (17)$$

And the total efficiency n_{tot} of the heat transfer surface is given by

$$n_{\mathrm{tot}} = 1 - \frac{A_{\mathrm{f}}}{A}(1 - n_{\mathrm{fin}}) \quad (18)$$

7.3 Compressors

Two compressors are installed in the experimental setup and are manufactured by GEA Bock. The 1st stage, low pressure compressor (RKX26/31-2 CO2 T) is a two pole type compressor with a swept volume of 5.4 m^3/h. The 2nd stage high pressure compressor (RKX26/31-4 CO2 T) used in two-stage compression mode applications is a four pole compressor with a swept volume of 2.7 m^3/h. The minimum and maximum mass flow rates according to the manufacturer for both compressors are 150 and 450 kg/h, respectively. The minimum limit is to ensure sufficient cooling of the hardware. The maximum operating pressure is 130 bar for both compressors. The maximum allowed discharge temperature is 160 °C for both compressors. A very small amount of the oil used for lubrication will leak out into the refrigerant which the system must remove and transfer back to the compressor to ensure proper levels of oil are maintained.

No mass flow meter is installed in the test setup. However, the mass flow at the inlet to each cycle component is constant in steady-state mode. The mass flow can therefore be estimated by analysis of an individual cycle component. In order to obtain an initial guess for the mass flow in the system, three different methods were initially chosen.

One method is to consider either the gas cooler or evaporator as a closed system and perform an energy balance of the system. The mass flow can then be calculated by

$$\dot{m} = \frac{\dot{Q}}{(H_{\mathrm{out}} - H_{\mathrm{in}})} \quad (19)$$

where the energy transfer in the system was found from the measured values for air with

$$\dot{Q} = V_{\mathrm{air}} A \left(\rho c_{\mathrm{p}}\right)_{\mathrm{air}} \Delta T_{\mathrm{air}} \quad (20)$$

In this equation V_{air} is the air velocity and A is the cross-sectional area of the heat exchanger unit perpendicular to airflow. Both properties are evaluated at the inlet to the air side of the heat

exchanger units. Due to the uncertainties regarding the distribution of refrigerant flow in the evaporator, the measured values for heat transfer of the refrigerant side in the evaporator were inconsistent. Therefore the energy balance was calculated using the gas cooler unit.

The other two methods for calculating the mass flow involve the volumetric efficiency, with the equation

$$\dot{m} = \rho_{\mathrm{in}} V_{\mathrm{s}} \eta_{\mathrm{v}} \frac{N}{60} \qquad (21)$$

Where the efficiency can be predicted from manufacturer data for the 1st stage compressor with

$$\eta_{\mathrm{v}} = 1.0609 - 0.1391\beta \qquad (22)$$

or an empirical model from Ortiz (2003)

$$\eta_{\mathrm{v}} = 0.9207 - 0.0756\beta + 0.0018\beta^2 \qquad (23)$$

Properties were obtained using REFPROP software and the measured temperature and pressure values.

With the mass flow calculated from one of the three methods above, the total efficiency was calculated by equation (24) below to check if the calculated values agreed to the manufacturer data from equation (25)

$$n_{\mathrm{tot}} = \dot{m} \frac{\left(H_{\mathrm{out,is}} - H_{\mathrm{in}} \right)}{\dot{W}_{\mathrm{meas}}} \qquad (24)$$

$$n_{\mathrm{tot}} = -0.0941\beta^2 + 0.5147\beta - 0.1736 \qquad (25)$$

As discussed later in the Results section, all three methods resulted in similar calculated values for $\dot{m}$ for all steady state test data. For comparison of the total efficiency correlations, Figure 15 is presented. In the figure, the calculated n_{tot} values from the method using equations (21), (22) and (24) matched relatively well with the predictions given from the manufacturer, equation (25).

Similar agreement was obtained using the other two mass flow calculation methods. Based on the agreement shown in Figure 15, it was assumed that the volumetric efficiency from manufacturer data, equation (22), also agreed to an acceptable extent. Equations (21) and (22) were therefore used in the model to calculate the refrigerant mass flow.

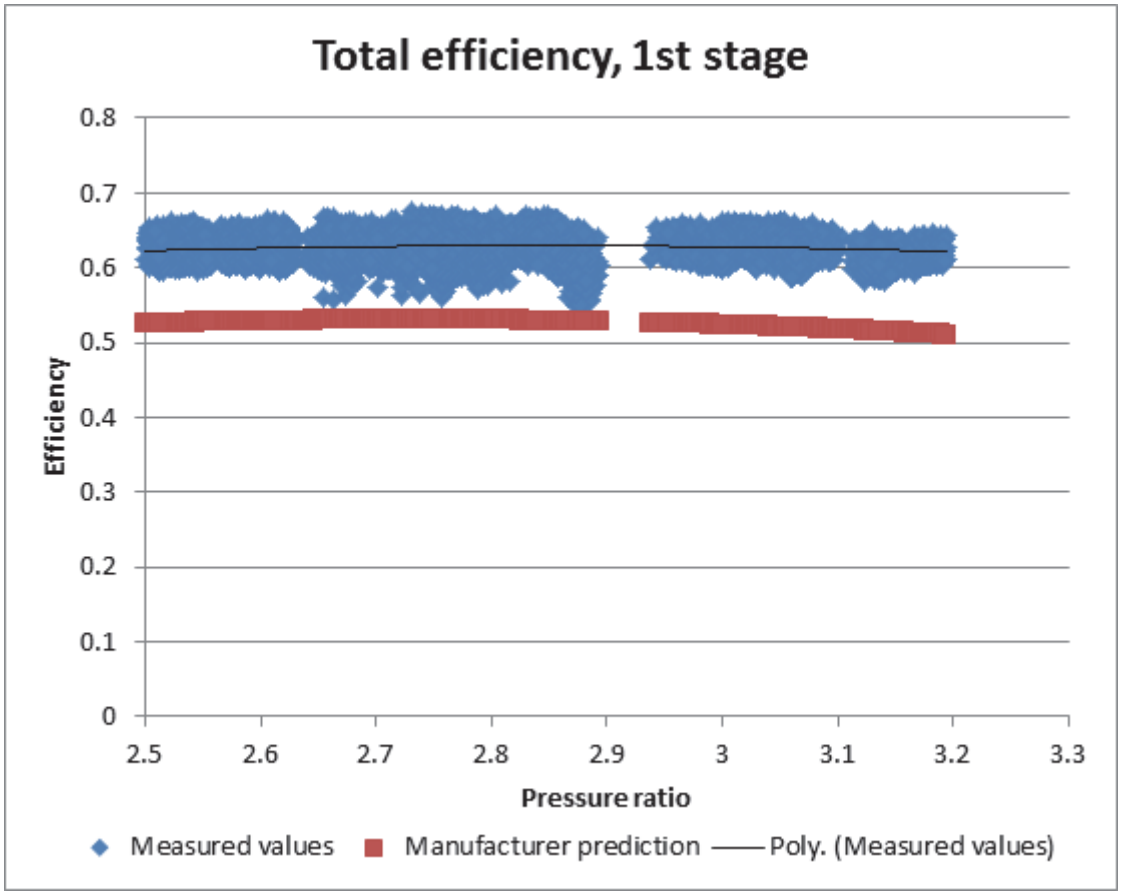

Figure 15. Efficiency comparison for first stage compressor in steady state operation compared to manufacturer data.

7.3.1 First stage

The correlations for the 1st stage compressor were used for mass flow calculations because the 2nd stage compressor efficiency equations were developed for single stage compression. The predicted efficiencies from both Ortiz (2003) and the compressor manufacturer also did not match the values calculated from measurement data obtained for this report. It was also believed that the 2nd stage compressor frequently overheated in previous tests at SP under normal operating conditions, resulting in calculation errors using existing correlations.

To find the mechanical plus electrical efficiency, the isentropic efficiency was calculated with measured values from

$$n_{\mathrm{is}} = \frac{H_{\mathrm{out,is}} - H_{\mathrm{in}}}{H_{\mathrm{out}} - H_{\mathrm{in}}} \qquad (26)$$

Using equations (24) and (26) the combined mechanical and electrical efficiency was then estimated by

$$n_{\mathrm{mech,el}} = \frac{n_{\mathrm{tot}}}{n_{\mathrm{is}}} \qquad (27)$$

This mechanical and electrical efficiency was used to calculate the real work done by the compressors. However, no manufacturer data exists for expected values, and therefore the error in the calculated values could not be analysed. Therefore, the actual $n_{\mathrm{mech,el}}$ used in the model was assumed to be a constant value for all pressure ratios and was estimated from measured steady-state data.

For the model, η_{v} and n_{tot} were calculated from equations (22) and (25), respectively. An efficiency curve was developed for η_{is} for the 1st stage compressor using the calculated η_{is} values from steady-state measured data.

$$n_{\mathrm{is,1st}} = 0.5439\beta^3 - 4.4405\beta^2 + 12.085\beta - 10.392 \qquad (28)$$

Outlet enthalpy of the 1st stage compressor was then be calculated by rearranging equation (26). The REFPROP program could then be used to determine the outlet temperature for the calculated pressure and enthalpy

7.3.2 Second stage

The calculated isentropic and total efficiencies for the 2nd stage compressor measured data did not match with manufacturer predictions. For the total efficiency, these poor matching results can be seen in Figure 16.

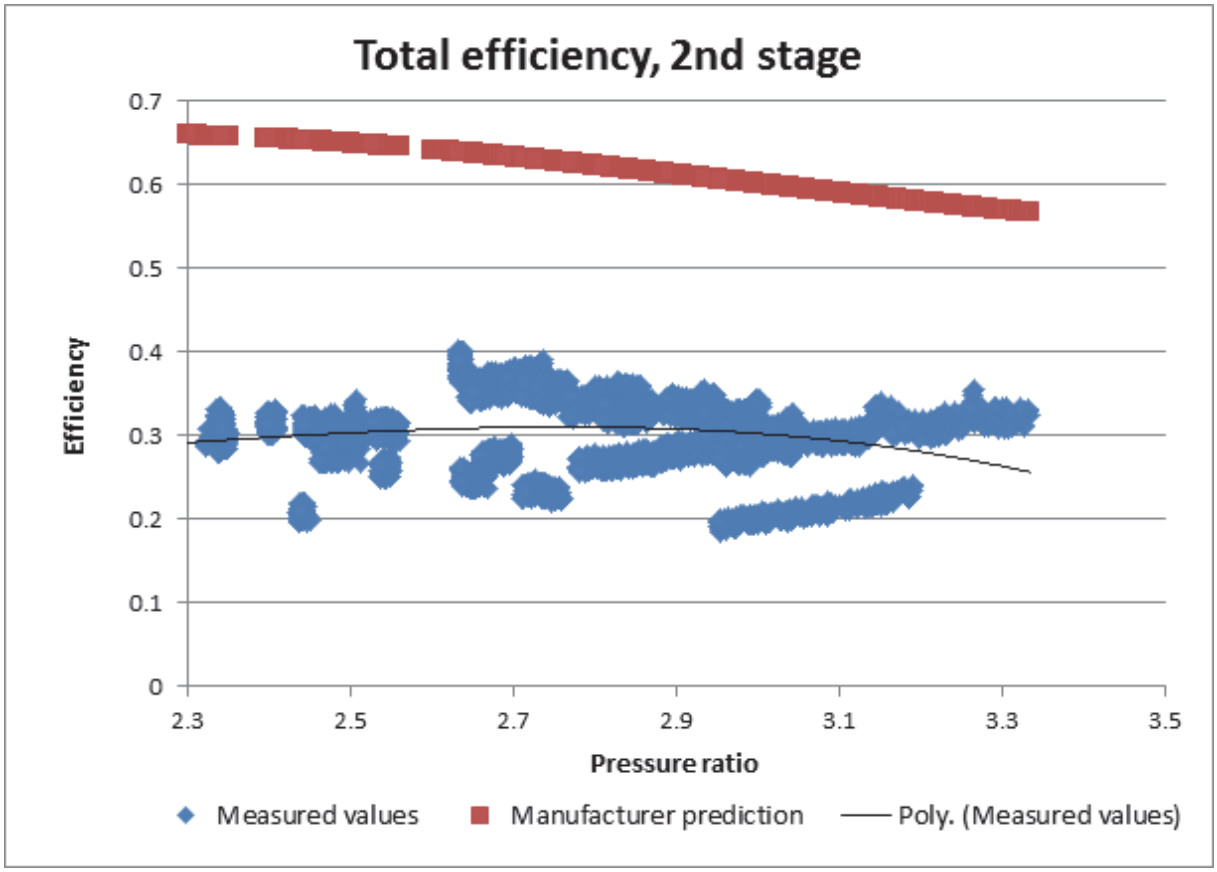

Figure 16. Efficiency comparison for first stage compressor in steady state operation compared to manufacturer data.

Due to the poor prediction of η_{is} and n_{tot} from manufacturer and theoretical data, efficiency curves were developed for both η_{is} and n_{tot} for the 2nd stage compressor model using the calculated values from measurement data. Isentropic efficiency values were calculated using equation (26). Total efficiency values were calculated using equation (24) and the calculation mass flow from equation (21).

$$n_{\mathrm{is,2nd}} = -0.0778\beta^3 + 0.5233\beta^2 - 1.0878\beta + 1.1937 \quad (29)$$

$$n_{\mathrm{tot,2nd}} = -0.0763\beta^3 + 0.5107\beta^2 - 1.0748\beta + 0.99 \quad (30)$$

As with the 1st stage compressor, the outlet conditions of the 2nd stage compressor were calculated by rearranging equation (26) with the calculated $n_{\mathrm{is,2nd}}$.

Although the calculated efficiencies varied significantly between tests, equations (29) and (30) were used due to the high error from using manufacturer and theoretical curves. Also, due to both shortages of accurate data and errors in the mass flow predictions, the mechanical and electrical efficiencies are assumed to be the same for the 2nd stage compressor as for the 1st stage compressor.

7.4 Gas cooler

Supercritical CO_2 enters the gas cooler after the first compressor in one-stage compression mode or after the second compressor in two-stage compression mode. Before entering the gas cooler, the CO_2 is divided into 4 tubes, resulting in some pressure losses. To simplify the model, it is assumed that the CO_2 is evenly distributed throughout each of the tubes.

Each of the 4 tubes passes through the gas cooler 22 times with pass lengths of 0.82 m. Figure 17 below shows a side view of the existing gas cooler configuration. The smaller unit at the bottom of the figure is the intermediate cooler which has 4 tubes and 6 passes, with pass lengths of 0.82 m. When the setup is run in one-stage compression mode the refrigerant flow bypasses the intermediate cooler and 2nd stage compressor, and is led directly into the gas cooler unit.

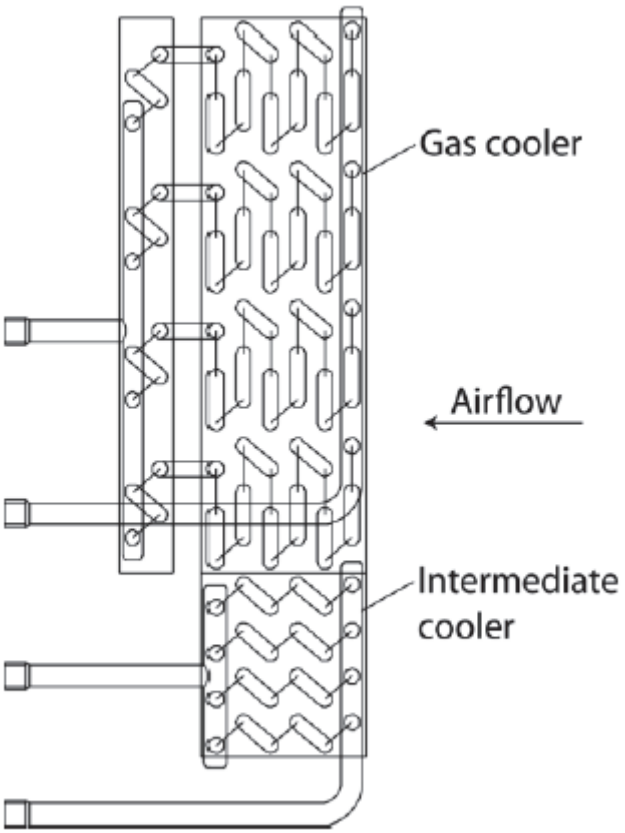

Figure 17. Side view of gas cooler and intercooler units in experimental setup (Jardeby, 2012).

7.4.1 Heat transfer

The heat transfer is calculated in the same way for both the intermediate cooler and the gas cooler, but with different heat transfer coefficient correlations.

As discussed in the Properties of CO_2 section, the thermo-physical properties of CO_2 vary widely as the temperature approaches T_{pc}, the pseudo-critical temperature. In the experimental setup the pseudo-critical temperature is relevant only for the heat transfer modelling in the gas cooler because this is the only heat exchanger component where the CO_2 is supercritical due to the high temperature and pressure.

The pseudo-critical temperature can be estimated with the correlation given by (B. T. Austin, 2011),

$$T_{\mathrm{pc}} = -31.4 + 12.15P - 0.6927P^2 + 0.0316P^3 - 0.0007521P^4 \qquad (31)$$

Where the unit of P is MPa.

Correlations of Nu are commonly used to account for the CO_2 property variations around T_{pc} when calculating the heat transfer coefficient of supercritical CO_2. For this report, the correlation of (S. H. Yoon et. al, 2003) is used, where

$$\mathrm{Nu_b} = a\mathrm{Re_b}^{b}\mathrm{Pr_b}^{c}\left(\frac{\rho_{\mathrm{pc}}}{\rho_{\mathrm{b}}}\right)^{n} \qquad (32)$$

$$T_{\mathrm{b}} > T_{\mathrm{pc}}: \quad a = 0.14, \quad b = 0.69, \quad c = 0.66, \quad n = 0$$

$$T_{\mathrm{b}} \le T_{\mathrm{pc}}: \quad a = 0.013, \;\; b = 1.0, \quad c = -0.05, \;\; n = 1.6$$

The heat transfer coefficient is then calculated by

$$h_{\mathrm{r}} = \frac{\mathrm{Nu}_{\mathrm{b}} k_{\mathrm{b}}}{D_{\mathrm{i}}} \qquad (33)$$

For the intermediate cooler, equation (33) is also used but the Nusselt number is calculated using the Dittus-Boelter equation

$$\mathrm{Nu} = 0.023 \mathrm{Re}^{0.8} \mathrm{Pr}^{\mathrm{n}} \qquad (34)$$

Where n is 0.3 for cooling and 0.4 for heating. This equation has been confirmed experimentally for the range of conditions

$$0.6 \lesssim Pr \lesssim 160$$

$$Re \gtrsim 10000$$

$$\frac{L}{D} \gtrsim 10$$

To calculate the heat transfer in the model the tubes are divided into small segments for each pass within the heat exchanger unit, giving a small amount of heat transfer per segment. The total heat transfer of all segments in one pass is then used to calculate the new average temperature of the air for that pass for the next iteration of the model, as explained above in the Air side part of the Model methodology section.

The refrigerant heat transfer coefficient is used to calculate the theoretical heat transfer from CO_2 to the air side in each segment by

$$\dot{Q}_{\mathrm{r,seg}} = h_{\mathrm{r}} A_{\mathrm{f}} (T_{\mathrm{w}} - T_{\mathrm{air}}) \qquad (35)$$

Where the surface area, A_{f}, is the tube internal surface area for the segment, T_{w} is evaluated at the inlet of the segment, and T_{air} is the temperature of the air over the entire pass. Similarly, the air side heat transfer coefficient is used to calculate the theoretical air side heat transfer by

$$\dot{Q}_{\mathrm{air,seg}} = h_{\mathrm{air}} A_{\mathrm{f}} (T_{\mathrm{w}} - T_{\mathrm{air}}) \qquad (36)$$

Where the surface area, A_{f}, is the exposed surface area of the tubes within the segment.
The actual heat transfer for each segment, $\dot{Q}_{\mathrm{seg}}$, is then dependant on whether the refrigerant or air side limits the amount of heat that can be transferred, including the heat transfer from the fins as explained in the Fins section above.

$$\dot{Q}_{\mathrm{seg}} = \min(\dot{Q}_{\mathrm{r,seg}}, (\dot{Q}_{\mathrm{air,seg}} + \dot{Q}_{\mathrm{fin}})) \qquad (37)$$

The refrigerant inlet temperature to the next segment is then calculated by calling REFPROP for the current segment outlet pressure and the outlet enthalpy calculated by

$$H_{\text{out,seg}} = H_{\text{in,seg}} - \frac{\dot{Q}_{\text{seg}}}{\dot{m}} \quad (38)$$

7.4.2 Pressure drop

Linear pressure drop of the supercritical CO_2 for each segment within the tubes is calculated with the Darcy–Weisbach equation

$$\Delta P = f \frac{L}{D_{\text{i}}} \frac{\rho V^2}{2} \quad (39)$$

Where the friction factor f depends on Re taken at the bulk of the fluid (F.P. Incropera et. al, 2007)

$$f = \begin{cases} \dfrac{0.316}{\text{Re}_{\text{b}}{}^{1/4}} & \text{for } \text{Re}_{\text{b}} < 2.0 \times 10^4 \\ \dfrac{0.184}{\text{Re}_{\text{b}}{}^{1/5}} & \text{for } \text{Re}_{\text{b}} \geq 2.0 \times 10^4 \end{cases} \quad (40)$$

And velocity is calculated by

$$V = \frac{\dot{m}}{\rho A_{\text{c}}} \quad (41)$$

The pressure drop of the supercritical CO_2 within the bends of the tube is calculated with

$$\Delta P = f \frac{8\dot{m}^2}{\pi^2 D_{\text{i}}{}^4 \rho} \quad (42)$$

Where the friction factor f depends on Re taken at the bulk of the fluid and is calculated by the Filonenko correlation

$$f = \frac{1}{(1.82\log(\text{Re}_{\text{b}}) - 1.64)^2} \quad (43)$$

For

$$1.0 \times 10^4 < \text{Re}_{\text{b}} < 5.0 \times 10^6$$

Outside this range of Re the Blasius correlation was used, where

$$f = \frac{0.316}{\text{Re}_{\text{b}}{}^{1/4}} \quad (44)$$

It should be noted that the bends have a slightly smaller inside diameter of 5.58 mm compared to the diameter of 6 mm in the straight tube sections.

7.5 Evaporator

Carbon dioxide is expanded in an expansion valve after the gas cooler. This CO_2 then enters the evaporator as a mixture of liquid and vapour. Here, as is common in most studies, the expansion process is assumed to be isenthalpic to simplify calculations for the mixture enthalpy and quality into the evaporator.

Before entering the evaporator the CO_2 is divided into 9 tubes, resulting in some pressure losses. To simplify the model, it is assumed that the CO_2 is evenly distributed throughout each of the 9 tubes. This assumption will be discussed further in the Discussion section of this report.

Each of the 9 tubes passes through the evaporator 10 times with pass lengths of 1.05 m. After the last pass the flow of CO_2 from all tubes is recombined back into one tube. Figure 18 below shows a side view of the existing evaporator configuration. The dotted lines demonstrate the distribution process into the 9 smaller tubes at the inlet of the evaporator.

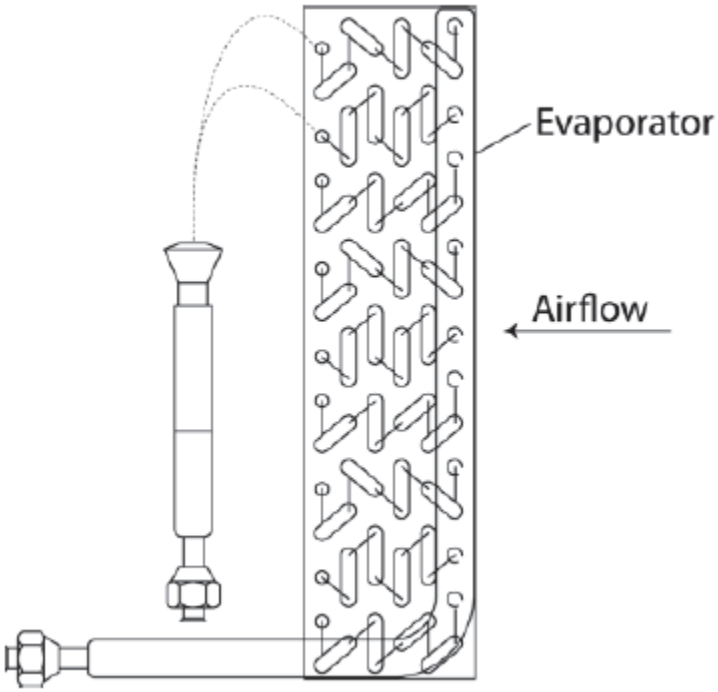

Figure 18. Side view of evaporator unit in experimental setup (Jardeby, 2012).

7.5.1 Heat transfer

Similar to the gas cooler and intercooler, the tubes and passes are divided into small segments in the evaporator. The heat transfer is calculated for each segment where the smaller of the air side potential heat transfer and the refrigerant side potential heat transfer determines the actual heat transfer for the current segment. Unlike the gas cooler and intercooler, flow in the evaporator is in both liquid and vapour phases and the heat transfer coefficient correlations for both flow types must be used.

7.5.1.1 Two-phase region

The model first uses REFPROP to calculate the inlet quality to the evaporator based upon the calculated CO_2 enthalpy out of the gas cooler, and isenthalpic expansion to a desired pressure level.

Then the total refrigerant heat transfer coefficient in each segment is calculated by

$$h_{\mathrm{r}} = h_{\mathrm{nb}} + h_{\mathrm{bc}} \tag{45}$$

Where h_{nb} is the nucleate boiling heat transfer coefficient and h_{bc} is the convection heat transfer coefficient. The model uses the correlation given by (Hwang Y., 1997) where

$$h_{\mathrm{nb}} = 0.00122\left(\frac{{k_{\mathrm{l}}}^{0.79}{c_{\mathrm{p,l}}}^{0.5}{\rho_{\mathrm{l}}}^{0.49}}{\sigma^{0.6}{\mu_{\mathrm{l}}}^{0.29}{H_{\mathrm{lv}}}^{0.24}{\rho_{\mathrm{v}}}^{0.24}}\right)\left(T_{\mathrm{w}} - T_{\mathrm{sat}}(P_{\mathrm{l}})\right)^{0.4}(P_{\mathrm{sat}}(T_{\mathrm{w}}) - P_{\mathrm{l}})^{0.75}S \tag{46}$$

$$h_{\mathrm{bc}} = h_{\mathrm{l}}{\mathrm{Pr}_{\mathrm{l}}}^{0.6}F(1-x)^{0.8} \tag{47}$$

The heat transfer coefficient for the liquid phase, h_{l}, is calculated by the Dittus-Boelter correlation

$$h_{\mathrm{l}} = \frac{\mathrm{Nu}k_{\mathrm{l}}}{D_{\mathrm{i}}} \tag{48}$$

$$\mathrm{Nu} = 0.023{\mathrm{Re}_{\mathrm{l}}}^{0.8}{\mathrm{Pr}_{\mathrm{l}}}^{0.4} \tag{49}$$

The coefficients S and F are calculated by

$$F = \begin{cases} 1 & \text{for } X_{\mathrm{tt}} \geq 10 \\ 2.0\left(0.213 + {X_{\mathrm{tt}}}^{-1}\right)^{0.736} & \text{for } X_{\mathrm{tt}} < 10 \end{cases} \tag{50}$$

Where the Martinelli number X_{tt} is given by

$$X_{\mathrm{tt}} = \left(\frac{1-x}{x}\right)^{0.9}\left(\frac{\rho_{\mathrm{v}}}{\rho_{\mathrm{l}}}\right)^{0.5}\left(\frac{\mu_{\mathrm{l}}}{\mu_{\mathrm{v}}}\right)^{0.1} \tag{51}$$

And

$$S = \frac{1 - \exp\left(\frac{-Fh_{\mathrm{l}}X_0}{k_{\mathrm{l}}}\right)}{\frac{Fh_{\mathrm{l}}X_0}{k_{\mathrm{l}}}} \tag{52}$$

Where

$$X_0 = 0.05\left(\frac{\sigma}{g(\rho_{\mathrm{l}} - \rho_{\mathrm{v}})}\right)^{0.5} \tag{53}$$

The heat transfer for each segment is then calculated by equation (35).

While the refrigerant is still in two-phase flow, heat transfer to the present segment acts to vaporize all or part of the remaining liquid refrigerant. In the model, the enthalpy for the next segment is then calculated by

$$H_{\mathrm{out,seg}} = H_{\mathrm{in,seg}} + \frac{\dot{Q}_{\mathrm{r,seg}}}{\dot{m}} \quad (54)$$

The model then uses REFPROP to calculate the inlet quality to the next segment using the calculated outlet enthalpy and pressure for CO_2 of the present segment. This two-phase heat transfer segment of the model is iterated until the quality reaches one; the condition where the flow is fully evaporated.

7.5.1.2 Single phase region

Heat transfer for each segment in the single phase vapour region of the evaporator is calculated by equations (33) and (35) to (38), as in the gas cooler and intercooler, but with one notable exception. Here, the Gnielinski correlation is used to calculate the Nusselt number for CO_2 in the single phase where

$$\mathrm{Nu_b} = \left(\frac{\left(\frac{f}{8}\right)(\mathrm{Re_b} - 1000)\mathrm{Pr_b}}{\left(1 + 12.7\left(\frac{f}{8}\right)^{0.5}\left(\mathrm{Pr_b}^{\frac{2}{3}} - 1\right)\right)} \right) \quad (55)$$

The friction factor f depends on Re taken at the bulk of the fluid and is calculated by the Filonenko correlation, equation (43).

7.5.2 Pressure drop

Similar to the gas cooler and intercooler, the pressure drop in the evaporator is calculated for each segment. However, linear pressure drop of the CO_2 within the evaporator tubes is more complex than that within the gas cooler due to the two-phase flow region.

7.5.2.1 Two-phase region

In the two-phase region, pressure drop is calculated in the model using the Friedel correlation. Pressure drop with this correlation is calculated by multiplication of the pressure drop for either the liquid, ΔP_{lo}, or the vapor, ΔP_{vo}, by its corresponding two-phase multiplier, Φ_{lo} or Φ_{vo}, respectively. The pressure drop calculated in the model is therefore

$$\Delta P_{\mathrm{f}} = \Delta P_{\mathrm{lo}} \Phi_{\mathrm{lo}} \quad (56)$$

The liquid only pressure drop is calculated by

$$\Delta P_{\mathrm{lo}} = f_{\mathrm{lo}} \left(\frac{2G^2}{D\rho_{\mathrm{l}}} \right) \quad (57)$$

Where the liquid only friction factor f_{lo} is defined by

$$f_{\mathrm{lo}} = \begin{cases} \dfrac{16}{\mathrm{Re_{lo}}} & \text{for } \mathrm{Re_{lo}} < 1055 \\ \dfrac{0.079}{\mathrm{Re_{lo}}^{1/4}} & \text{for } \mathrm{Re_{lo}} \geq 1055 \end{cases} \quad (58)$$

The two-phase multiplier is

$$\Phi_{\mathrm{lo}}{}^2 = E + \left(\frac{3.23FH}{\mathrm{Fr}^{0.045}\mathrm{We}^{0.035}}\right) \quad (59)$$

With the dimensionless coefficients as follows

$$E = (1-x)^2 + x^2 \frac{\rho_{\mathrm{l}} f_{\mathrm{vo}}}{\rho_{\mathrm{v}} f_{\mathrm{lo}}} \quad (60)$$

$$F = x^{0.78}(1-x)^{0.224} \quad (61)$$

$$H = \left(\frac{\rho_{\mathrm{l}}}{\rho_{\mathrm{v}}}\right)^{0.91} \left(\frac{\mu_{\mathrm{v}}}{\mu_{\mathrm{l}}}\right)^{0.19} \left(1 - \frac{\mu_{\mathrm{v}}}{\mu_{\mathrm{l}}}\right)^{0.7} \quad (62)$$

Where the vapour only friction factor f_{vo} is given by

$$f_{\mathrm{vo}} = \begin{cases} \dfrac{16}{\mathrm{Re_{vo}}} & \text{for } \mathrm{Re_{vo}} < 2000 \\ \dfrac{0.079}{\mathrm{Re_{vo}}^{1/4}} & \text{for } \mathrm{Re_{vo}} \geq 2000 \end{cases} \quad (63)$$

And with the Froude and Weber number for two-phase flow

$$\mathrm{Fr} = \frac{G^2}{gD\rho_{\mathrm{tp}}{}^2} \quad (64)$$

$$\mathrm{We} = \frac{G^2 D}{\sigma \rho_{\mathrm{tp}}} \quad (65)$$

Where the homogenous two-phase density, ρ_{tp}, is calculated by

$$\rho_{\mathrm{tp}} = \left(\frac{x}{\rho_{\mathrm{v}}} + \frac{(1-x)}{\rho_{\mathrm{l}}}\right)^{-1} \quad (66)$$

The pressure drop in the tube bends for the two-phase refrigerant flow was calculated using the Geary correlation

$$\Delta P = f_{tp} \frac{L x^2 G^2}{2\rho_{\mathrm{v}} D_{\mathrm{i}}} \quad (67)$$

Where the two-phase friction factor is calculated by

$$f_{tp} = \frac{80352 \times 10^{-8} \times \mathrm{Re_v}^{0.5}}{x^{1.25} \exp\left(0.215 \frac{C_\mathrm{d}}{D_\mathrm{i}}\right)} \quad (68)$$

Where C_d is the centre-to-centre distance of the bend and D_i is the bend inside diameter. As with the intercooler and gas cooler, it should be noted that the bends in the evaporator have a slightly smaller inside diameter of 5.58 mm compared to the diameter of 6 mm in the straight tube sections. Due to a lack of exact measurements, some assumptions were made. The centre to centre distance for the bend, C_d, was estimated to be 4 times the length of the tube inside diameter. The length of the bend, L, was estimated to be half the circumference of a circle with a diameter of C_d.

7.5.2.2 Single phase region

As with the intercooler and gas cooler, the linear pressure drop of the vaporized CO_2 within the tubes is calculated using equations (39) to (41).

The pressure drop of the vaporized CO_2 within the bends of the tube is calculated using the same method as for the intercooler and gas cooler, equations (39) to (44).

7.6 Simplified empirical models of the heat exchanger units

Comparisons show that most of the theoretical calculations predict the actual heat transfer measured from the experimental setup quite poorly. Therefore, simplified empirical models based on measured data were created for both faster and more accurate modelling purposes.

7.6.1 Simple gas cooler and intermediate cooler models

Since both the intermediate cooler and the gas cooler were proven both in theory and practice to be over dimensioned for their purpose, simple models were created where the outlet tube wall temperature of the units was set to a temperature just above the inlet air temperature. Depending on the air inlet temperature, the total energy transferred and the outlet air temperature could then be calculated with known CO_2 mass flow, as well as inlet and outlet tube wall temperatures. The pressure drop was estimated from measured pressure drops in the previous test data. Since the actual pressure drop caused by the distributor is very hard to predict and the measured pressure drop only varied slightly between the tests done, an average value from measurement data was set as a constant pressure drop in the simple model.

7.6.2 Simple evaporator model

The theoretical model of the evaporator under-predicts the heat transfer by a factor of around two. Possible reasons for this will be mentioned later in the Discussion section of this report. Since both theory and practice shows that the air side limits the heat transfer in the evaporator, a given inlet temperature and a desired value of the outlet temperature of the air was set. Given those two values and the airflow, the total heat transferred could be calculated. If this calculated heat transfer was capable of fully evaporating the CO_2, the model moved on to the next step. If not, a warning was announced before the next step. This warning indicates that either too high mass flow was flowing through the system or that the expansion valve outlet pressure needed to be adjusted. The pressure drop was modelled in the same way as for the gas cooler, with the same motivation, by estimating an average value from test data.

8 Results

As an introduction to this section, an example of some measured and calculated work values along with air heat transfer from testing is attached in Table 1 below. All values in the table are steady-state average values for one day of testing. Compressor work values are the measured electrical work by the compressors. Fan work for the gas cooler and intercooler (GC and IC) is the combined work from both fans. Similarly, the fan work for the evaporator (EV) is the combined work from both evaporator fans. Air heat transfer values are the calculated values using constant heat capacity and flow rate and the measured air temperature difference.

Table 1. Comparison between the brine system measured data and calculated data based on air properties and measurements for five different steady-state operation occasions.

Run #	Compressor Work (W)		Fan Work (W)		Brine System (W)		Air Heat Transfer (W)	
	Low Pressure	High Pressure	GC and IC	EV	GC and IC	EV	GC and IC	EV
1	2378	3992	1133	1168	13093	5296	13596	6050
2	2408	3697	1126	1173	12957	5104	13553	5825
3	2460	3363	1129	1168	13018	5421	13664	6182
4	2325	4854	1141	1146	11808	4543	12045	5205
5	2431	4105	1128	1127	12740	4773	13263	5437

Table 1 above shows that there is a small difference between the air heat transfer measurements and the corresponding brine system measurements. This indicates a small leakage of the air in each heat exchanger, though there is also the possibility of some error with the assumption of perfectly-mixed air. The losses are also much higher for the evaporator heat exchanger unit than those for the gas cooler and intercooler unit. This is probably because of the lower temperature of the air surrounding the evaporator which leads to a higher degree of exchanging with the ambient air. It is also important to note that the test setup was designed to resemble a real system, and therefore the heat exchanger units are not completely sealed to prevent air leakage.

For calculations in the model, the brine system heat transfer measurement from the gas cooler and intercooler unit is split into separate values for the gas cooler and intercooler depending on the ratio of surface areas perpendicular to the incoming airflow.

8.1 Measurement data

Tests were conducted on the experimental setup to better understand the real operating conditions. Unless otherwise stated, all values used to create Figure 19 - Figure 26 were average values for each steady-state operating region within the test data measured during the months of March, April and May 2012 for two stage compression at nominal compressor speeds of 3000 and 1450 RPM for the 1st and 2nd stage respectively.

8.1.1 Refrigerant mass flow rate

In order to create a system model, a correlation must be used to predict the mass flow of CO_2 within the system. As described previously in the Compressors part of the Model methodology section, the mass flow was predicted from measured data in multiple ways. In Figure 19 below, mass flows were compared to those calculated by an energy balance in the gas cooler using the measured air heat transfer to the brine system. The first method was through an energy balance of the evaporator using the measured air heat transfer to the brine system (Brine, evaporator). The last two methods

are from calculations with the volumetric efficiency correlations from a study by Ortiz (2003) and from compressor manufacturer data (Manufacturer).

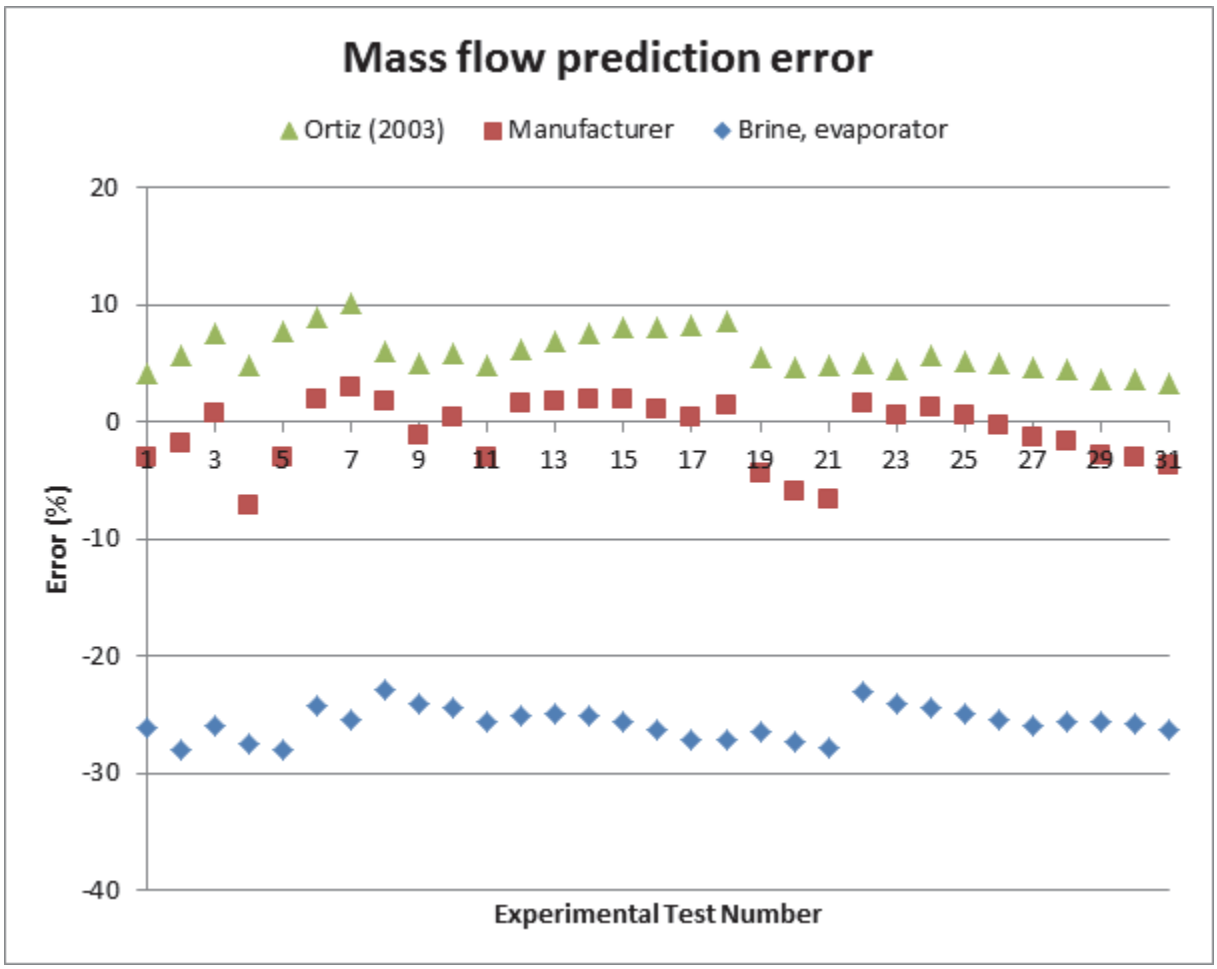

Figure 19. Error compared to calculated mass flow within the gas cooler.

Due to a lack of measurements as discussed in General model assumptions part of the Model methodology section, some assumptions were required to obtain the results in Figure 19 above. Temperature was measured at all times using thermocouples attached to the outside of the tubes and it was assumed that the wall temperatures were the same as the bulk temperatures. Perfect air mixing before the gas cooler and intercooler components was also assumed during steady-state operation. The analysis shows that there is some uncertainty in refrigerant mass flow calculations due to many assumptions. However, the general trend in Figure 19 shows that the calculated mass flow was similar for all methods except that of the evaporator brine system.

8.1.2 Refrigerant flow distribution

Tests were also conducted to determine the level of uneven distribution of CO_2 flow in the evaporator due to the unique distribution device installed. This was achieved by placing 5 thermocouples near the distributor device in the evaporator. The placement of the thermocouples can be seen in Figure 20. As seen in Figure 20, one thermocouple was placed on the larger tube immediately before the distributor, labelled later as Before Distributor in Figure 21. Three thermocouples were placed on the tube bends just before the entrance to the evaporator on the CO_2 side. The bends were chosen to maximize the distance between tubes measured, and are labelled as

Top Bend, Middle Bend and Bottom Bend in Figure 21. The last thermocouple was added about 2 cm after the distributor device to the same tube measured with the Top Bend thermocouple, and is labelled After Distributor in Figure 21.

Figure 20. A detailed view of the evaporator distributor showing the added thermocouples.

Figure 21 shows the average temperature distribution measurements for 29 different steady-state tests over 6 different testing periods, with the black vertical lines in the figure used to separate the different testing periods. It should be noted that although the test periods in Figure 21 are in chronological order and the tests are labelled from 1 to 29, there were additional tests that occurred between the testing periods that were omitted for simpler display purposes.

The first and last testing periods in the figure took place on two separate days and were for tests where the 2nd stage compressor rotational speed was changed after each steady-state test, as discussed later in the Results section. For test numbers 1 – 4 and 24 – 29, the 2nd stage compressor speed was decreased in uneven steps from 1450 rpm to 1100 rpm. All other manually variable conditions were kept as close as possible between those steady-state tests.

The other four testing periods shown in Figure 21 are from tests where the expansion valve outlet pressure was changed after each steady-state test, as discussed later in the Results section. For these four testing periods, the 1st and 2nd periods are from one test day, and the 3rd and 4th are from an

additional test day. For test numbers 5 - 10, the expansion valve outlet pressure was decreased between each steady state test in approximately even steps from about 17.8 to 16.0 bar. For test numbers 11 – 13, the pressure was decreased from about 15.7 to 15.0 bar. For test numbers 14 – 19, the pressure was decreased from about 17.5 to 15.75 bar. For test numbers 20 – 23, the pressure was decreased from about 16.7 to 15.5 bar. All other manually variable conditions were kept as close as possible between these steady-state tests.

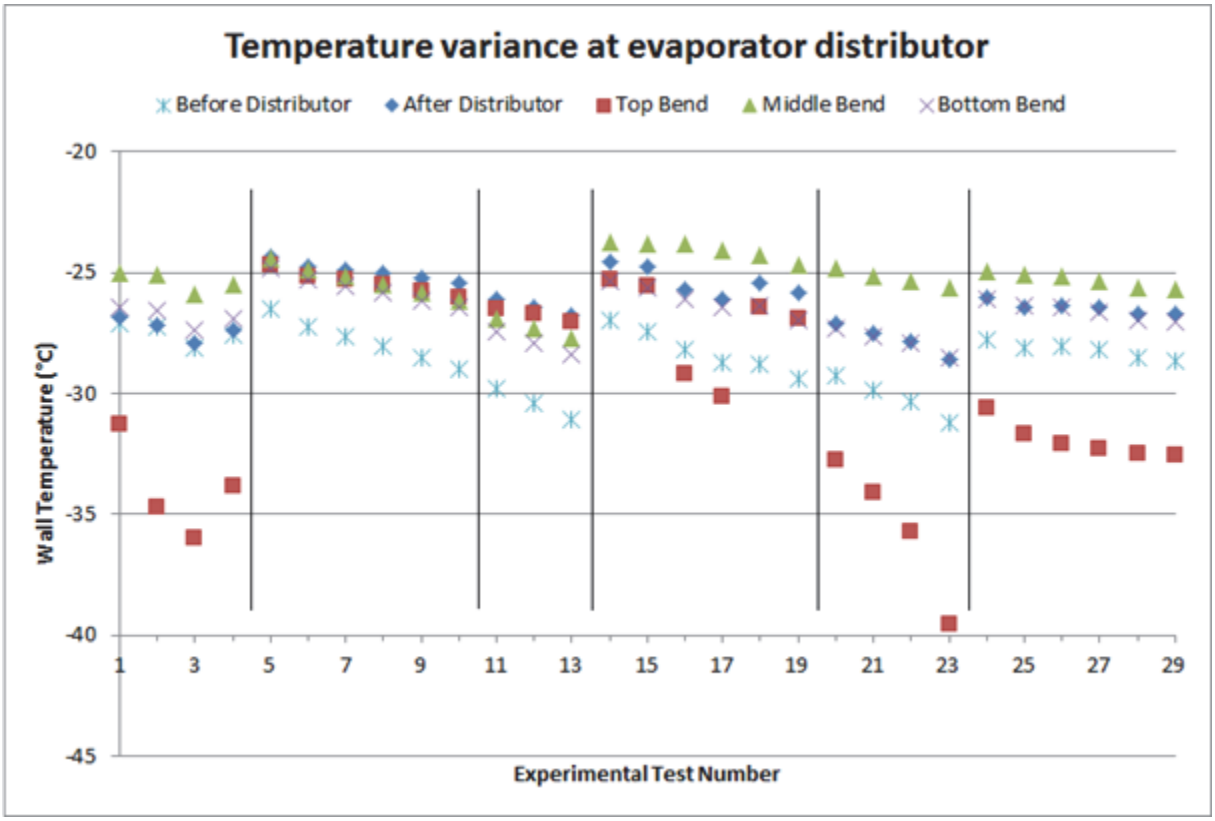

Figure 21. CO_2 flow maldistribution in two stage compression cycle at steady state.

As seen in Figure 21, the flow temperature is heavily dependent on both the tube studied and the test conditions. Since the thermocouples are well-insulated from outside air, it is assumed that the temperature differences shown above reflect significant refrigerant maldistribution within the tubes. As one example, despite being located on the same tube after the distributor, the thermocouples labelled After Distributor and Top Bend differed by 5°C or more in some measurements. From the figure it can be observed that the refrigerant distribution remained relatively constant throughout the tests conducted during the same test session, such as experimental test numbers 5-10. Overall, Figure 21 shows that the distribution within each tube cannot accurately be predicted without a more detailed and focused study using the experimental test setup.

8.1.3 Compressor performance

For the model to accurately predict compressor behaviour, the expansion valve outlet pressure was varied in the experimental setup with all remaining parameters kept constant. For all tests, the 1st and 2nd stage compressors were operated at speeds of 3000 and 1450 RPM, respectively. The compressor pressure ratios and outlet pressures were then studied to determine a pattern. The

results of this first session of test data are shown in Figure 22 below, where it can be seen that no clear pattern was observed in the data.

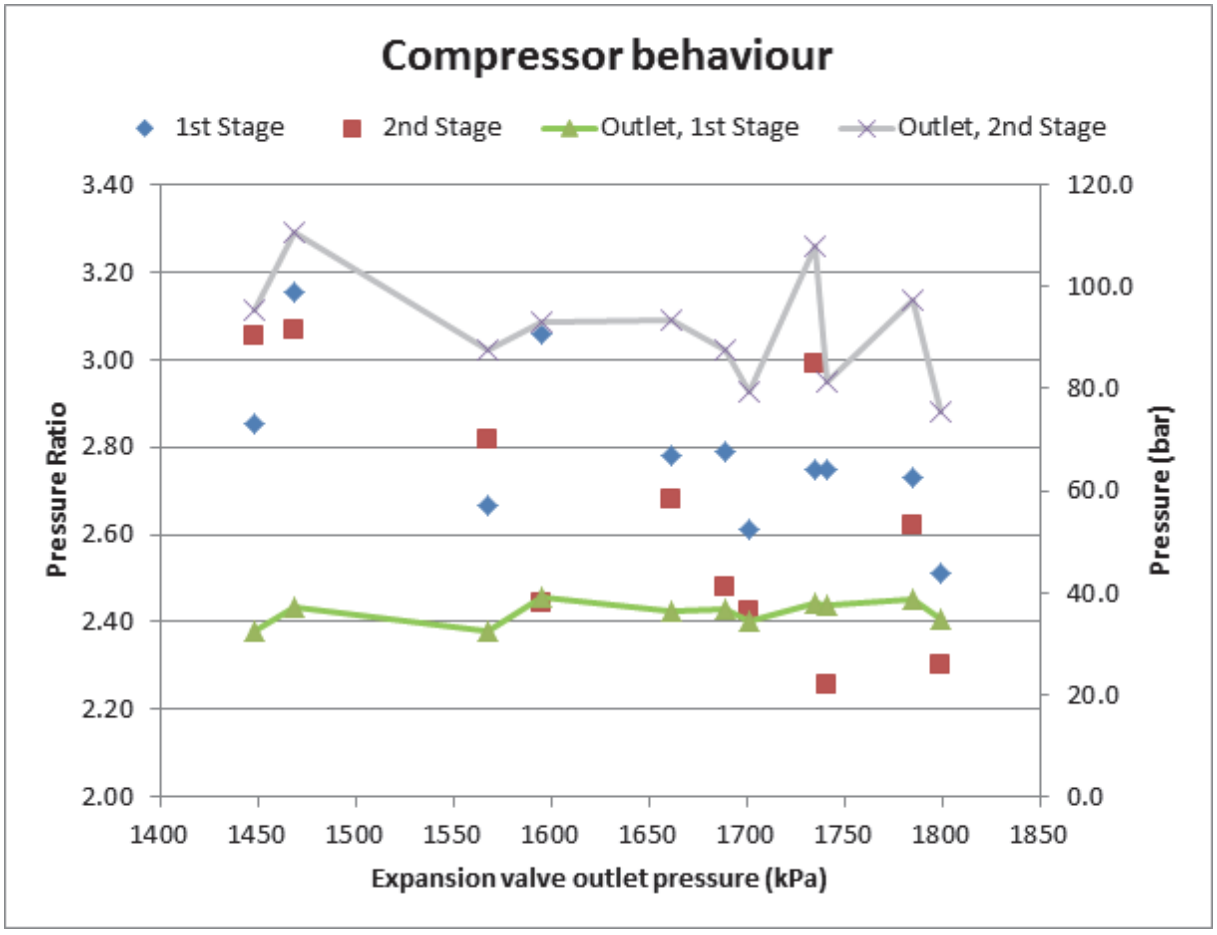

Figure 22. Compressor behaviour as a function of the expansion valve settings.

Additional tests were conducted at steady-state conditions to develop an overall prediction for the effects of expansion valve outlet pressure on the compressor behaviour, as seen in Figure 23 - Figure 26 below. As with the tests presented in Figure 22, the 1st and 2nd stage compressors were operated at speeds of 3000 and 1450 RPM, respectively, and all other parameters remained constant. For Figure 23 below, test sessions 2 and 3 were conducted on the same day. The first 3 data pairs are from the afternoon test session and the rest are in the morning. Similarly, test sessions 4 and 5 are from the same day with session 4 in the morning and session 5 in the afternoon. Sessions 4 and 5 are split into two figures for better visualization. When comparing all the data it can be seen that the 1st stage compressor pressure ratios were always lower than those of the 2nd stage compressor in the morning tests, but the opposite effect was observed in the afternoon tests.

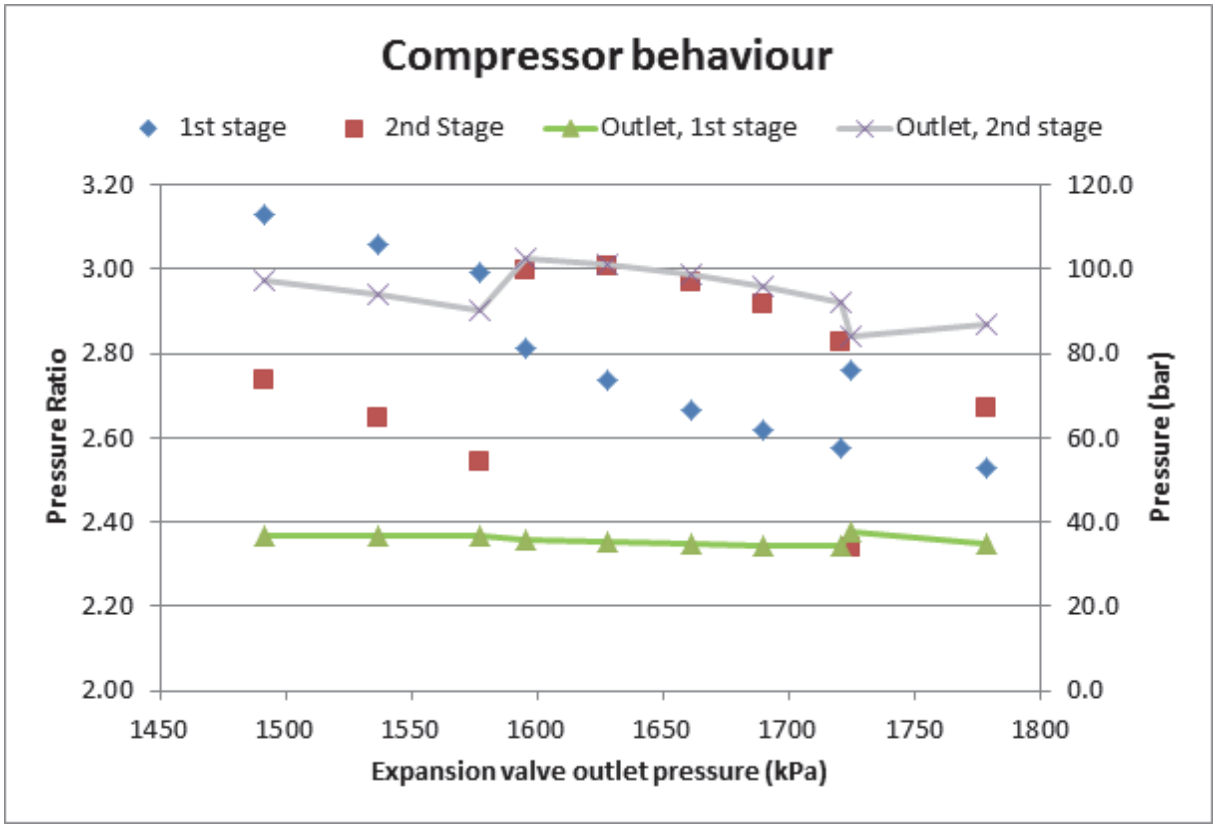

Figure 23. Compressor behaviour as a function of the expansion valve settings, test sessions 2 and 3.

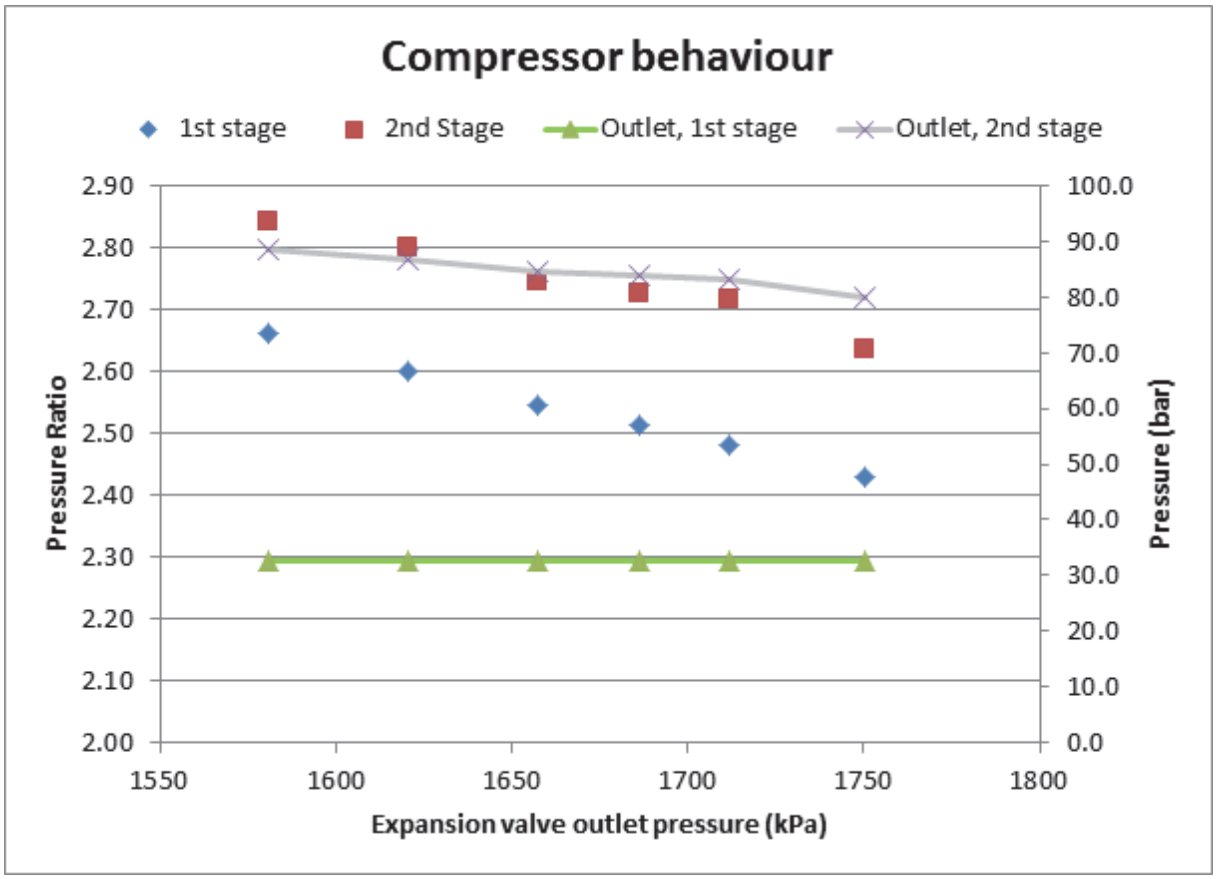

Figure 24. Compressor behaviour as a function of the expansion valve settings, test session 4.

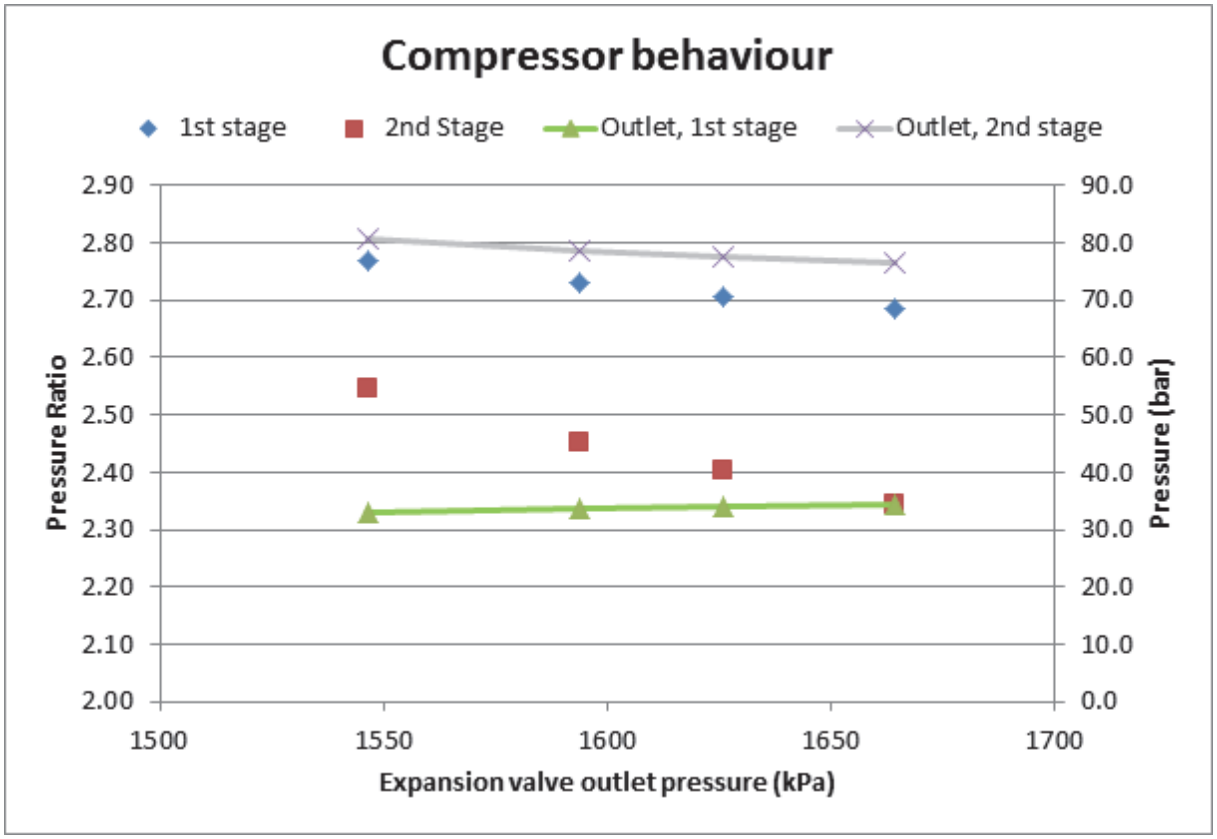

Figure 25. Compressor behaviour as a function of the expansion valve settings, test session 5.

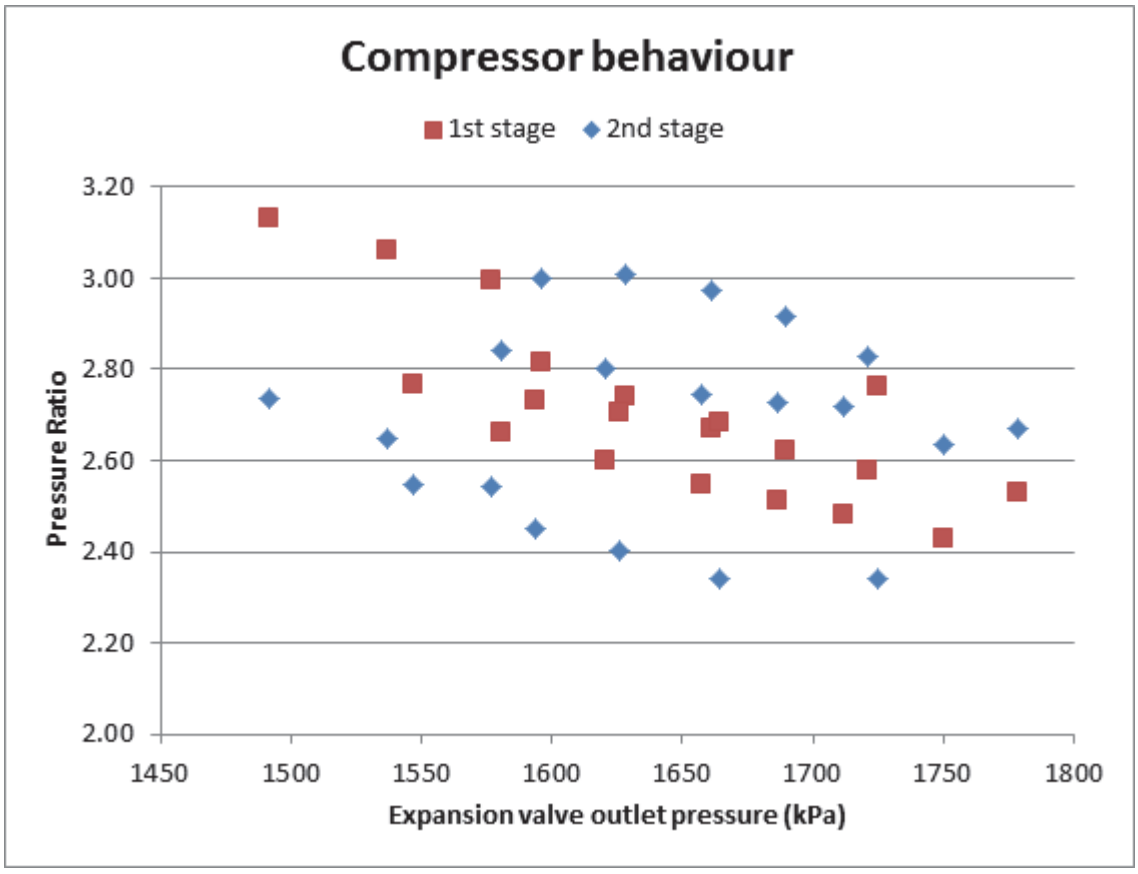

Figure 26. Combined data from test session 2 - 5.

Tests were also carried out over two separate days to determine system performance when operating the compressors at speeds other than those recommended by the compressor manufacturer. Frequency converters attached to the experimental setup were used to make these changes. The results of these tests are shown in Figure 27 below, where the superheat temperature in the evaporator was kept as constant as possible for all cases, around 8°C for all Day 1 tests, and around 11°C for all Day 2 tests. It was shown that overall performance can be increased significantly when operating the second stage compressor at the decreased speed of 1100 rpm while maintaining the first stage compressor speed of 3000 rpm.

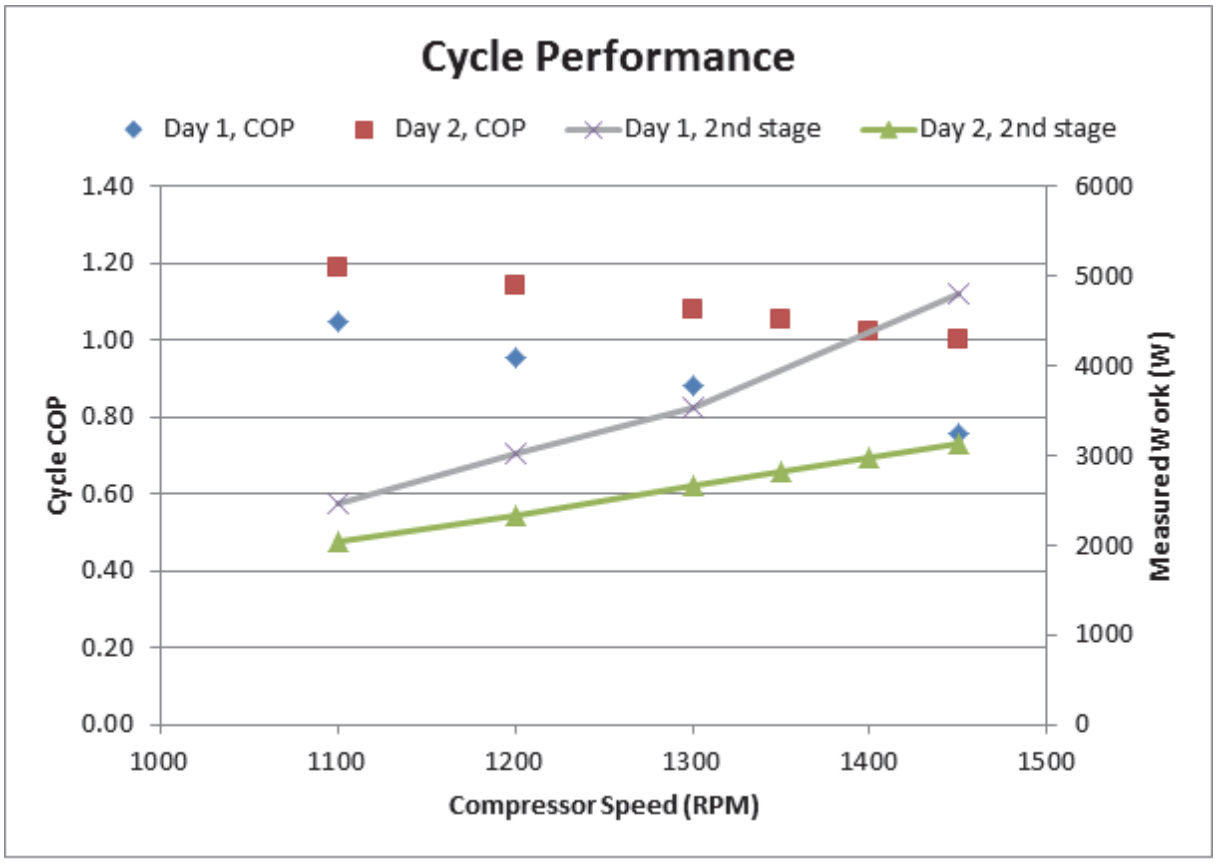

Figure 27. Cycle performance for variation in 2nd stage compressor speeds and constant 1st stage compressor speed.

8.2 Model results

To verify the accuracy of the model, several tests were done to determine the performance predictions at varying cycle conditions. First, the expansion valve outlet pressure was varied for different ambient temperatures, the results of which can be seen in Tables 1 through 4 below. In all four tables, data was calculated using assumed compressor speeds of 3000 RPM for the 1st stage and 1450 RPM for the 2nd stage. The superheat temperatures are around 10°C for all results shown in the tables below, which is very close to the air inlet temperature. This is further discussed in the Evaporator part of the Discussion section.

Since the heat pump system is intended for mobile applications where the gas cooler heat is rejected to the outside air, the COP values calculated for this report only consider the air cooling by the evaporator unit to be useful work. COP calculations from measurement data also use an

approximate value for fan work based upon the measurement data collected for all experiments. The model uses the equation

$$\mathrm{COP} = \frac{\dot{Q}}{\dot{W}_{\mathrm{fan}} + \dot{W}_{1\mathrm{st}} + \dot{W}_{2\mathrm{nd}}} \qquad (69)$$

where $\dot{Q}$ is the energy transferred from the air to the CO_2 over the evaporator and $\dot{W}_{1\mathrm{st}}$ and $\dot{W}_{2\mathrm{nd}}$ are the compressor work values.

Table 2. Performance of the model for an ambient temperature of 280 K.

Expansion valve outlet [kPa]	Mass flow [kg/s]	Q evaporator [W]	COP
1500	0,0257	5949	0,74
1540	0,0269	6226	0,77
1580	0,0283	6507	0,79
1620	0,0296	6792	0,82
1660	0,0309	7081	0,84
1700	0,0323	7375	0,87
1740	0,0338	7672	0,89
1780	0,0352	7973	0,91
1800	0,0360	8124	0,93

At this outside air temperature and above 1800 kPa expansion valve outlet pressure, the model predicts liquid CO_2 will remain in the tubes after the evaporator unit. Performance predictions are therefore not included in Table 2 above for valve outlet pressure above 1800 kPa. Expansion valve outlet pressure levels below 1500 kPa caused the 2nd stage compressor to overheat according to the model.

Table 3. Performance of the model for an ambient temperature of 285 K.

Expansion valve outlet [kPa]	Mass flow [kg/s]	Q evaporator [W]	COP
1520	0,0263	5756	0,70
1560	0,0276	6018	0,73
1600	0,0289	6284	0,75
1640	0,0303	6553	0,77
1680	0,0316	6825	0,79
1720	0,0331	7100	0,82
1760	0,0345	7379	0,84
1800	0,0360	7660	0,86
1840	0,0375	7944	0,88
1860	0,0382	8086	0,89

Similar to the results from Table 2, Table 3 shows that the model predicted liquid CO_2 after the evaporator unit for expansion valve outlet pressures above 1860 kPa and overheating of the 2nd compressor occurred at expansion valve outlet pressures below 1520 kPa. Compared to the results from Table 2, the COP of the cycle is lower for the higher ambient temperature in Table 3.

Table 4. Performance of the model for an ambient temperature of 290 K.

Expansion valve outlet [kPa]	Mass flow [kg/s]	Q evaporator [W]	COP
1600	0,0289	5888	0,69
1640	0,0303	6137	0,71
1680	0,0316	6388	0,73
1720	0,0331	6641	0,75
1760	0,0345	6895	0,77
1800	0,0360	7151	0,79
1840	0,0375	7408	0,81
1880	0,0390	7665	0,83
1920	0,0406	7922	0,85
1960	0,0422	8179	0,87

For the ambient temperature model results presented in Table 4, there is an enhanced effect of the results from Table 2 and Table 3. For the results presented in Table 4, above 1960 kPa expansion valve outlet pressure liquid CO_2 remains in the system after the evaporator unit and below 1600 kPa expansion valve outlet pressure, the 2nd compressor becomes overheated.

Table 5 shows results from a rather high ambient temperature of 298 K. At this ambient air condition, the model runs with an extra internal heat exchanger to prevent overheating in the 2nd stage compressor due to the high ambient temperatures.

Table 5. Performance of the model for an ambient temperature of 298 K, with an additional internal heat exchanger.

Expansion valve outlet [kPa]	Mass flow [kg/s]	Q evaporator [W]	COP
1500	0,0232	4166	0,54
1540	0,0244	4350	0,56
1580	0,0255	4534	0,57
1620	0,0267	4717	0,59
1660	0,0279	4898	0,61
1700	0,0291	5076	0,62
1740	0,0304	5251	0,64
1780	0,0317	5421	0,65
1820	0,0330	5584	0,66
1860	0,0343	5739	0,67
1900	0,0357	5880	0,68
1940	0,0370	6003	0,69
1980	0,0384	6095	0,69
2000	0,0392	6122	0,70

As can be seen in Table 5, according to the model the system COP is significantly reduced for sufficiently high ambient air conditions where an internal heat exchanger would be needed. However, the model results indicate also that a higher expansion valve outlet pressure is possible for

high ambient temperatures with an internal heat exchanger. Additionally, the lower limit for the expansion valve outlet pressure before overheating the 2nd compressor is relatively low and can be compared to the results from Table 2 for 280 K.

8.2.1 Example of model output figures

Examples of the graphical output from the model are presented in Figure 28 and Figure 29 below. The red line in each figure illustrates the saturation curve of CO_2 and the blue lines illustrate the cycle behaviour. The marked points shown are the locations before and after the different units in the cycle. In the report, it was chosen to show the Pressure-Enthalpy diagrams, though if desired a Temperature-Enthalpy diagram can be chosen when running the model.

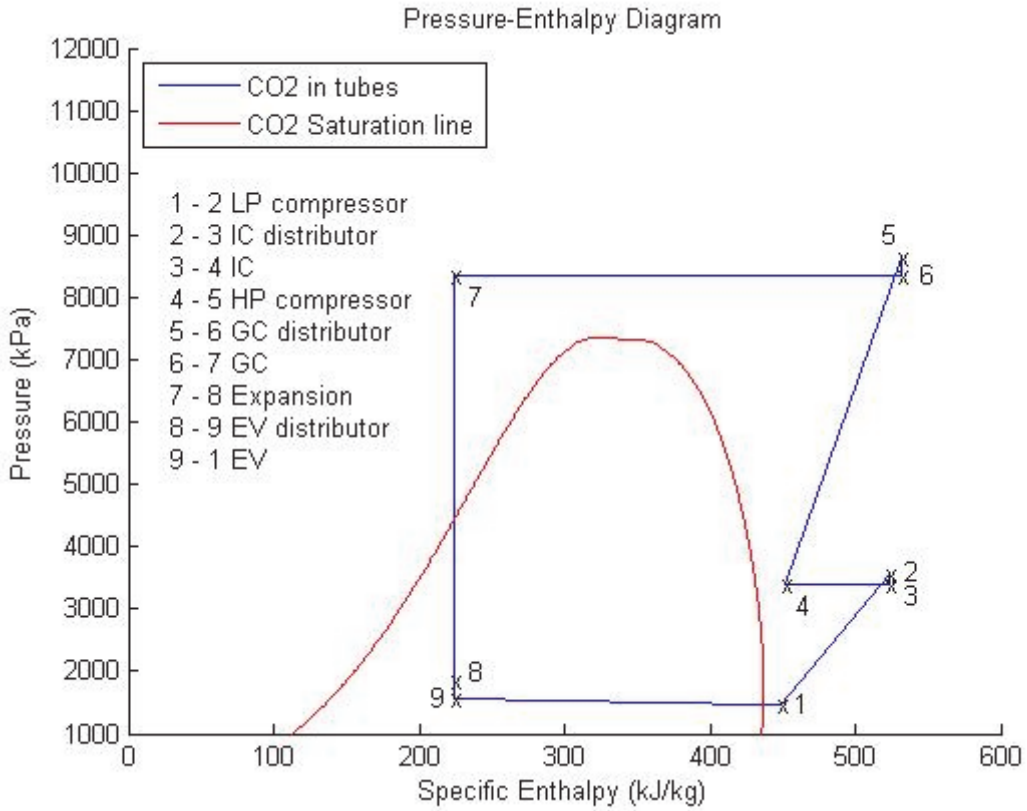

Figure 28. Example of model output for maximum COP with 280 K ambient temperature and compressor speeds of 3000/1450 RPM for the 1st and 2nd stage respectively.

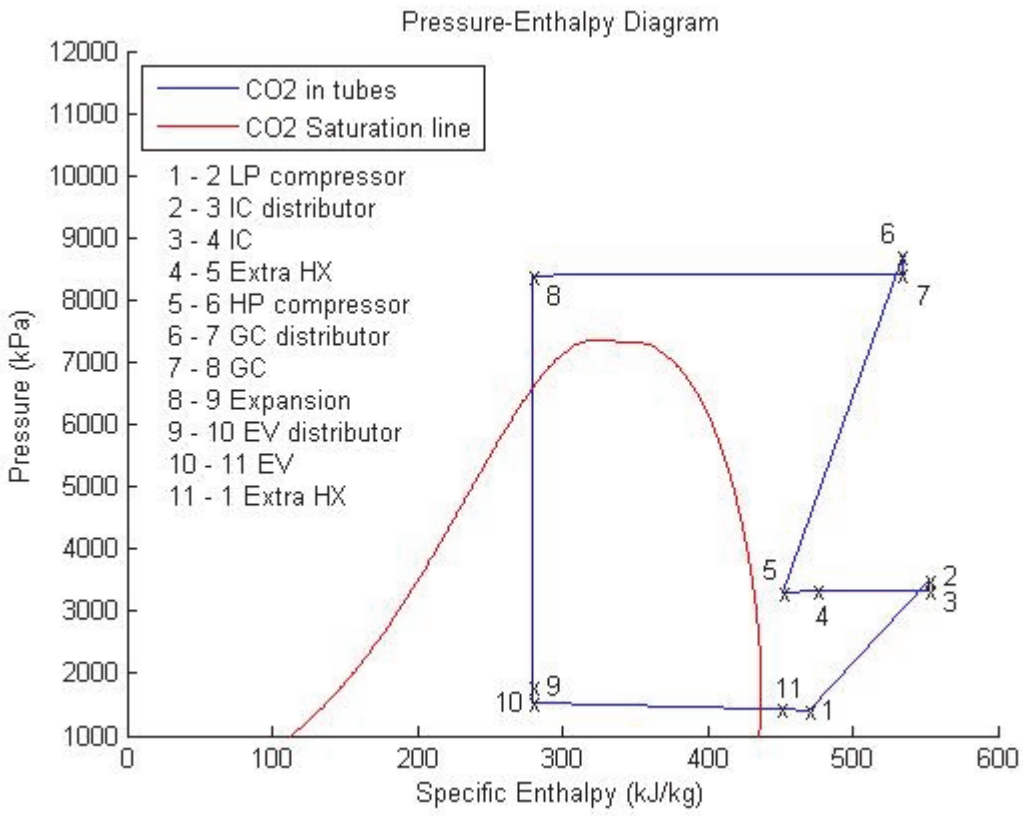

Figure 29. Example of model output for 298 K ambient temperature with internal heat exchanging, compressor speeds of 3000/1450 for the 1st and 2nd stage respectively.

9 Discussion

Many assumptions were required to analyse the measured data and to create the mathematical model. Additionally, from the Results section it can be seen that there are many interesting and unexpected results from the measured data. The significance of these assumptions and unexpected results will be presented here in the Discussion section.

9.1 Compressor

The first stage compressor was used for mass flow calculations because the calculated efficiencies for the 2nd stage compressor were significantly lower than expected from the manufacturer and theoretical correlations. No noticeable overheating was observed during the conducted tests. One likely explanation for the low efficiency results is that the high pressure compressor in the experimental setup was used as a 2nd stage compressor, whereas the manufacturer and theoretical correlations were developed with the compressor operating in a one-stage compression cycle.

Regarding the volumetric efficiency for the two compressors, the 2nd stage has half of the volumetric capacity as the 1st stage compressor even though the pressures are around 2.5-3 times higher for the 2nd stage. This could explain the poor behaviour of the 2nd stage compressor compared to manufacturer and theoretical predictions and needs to be further analysed. Another potential reason for the low 2nd stage efficiency could be that the frequency converter causes problems in the form of electrical inefficiency.

Another likely explanation is that the calculated refrigerant mass flow rate was lower than the minimum mass flow rate suggested by the manufacturer for both compressors to ensure motor cooling. From the measurement data, the calculated mass flow was typically about 100-125 kg/h during steady-state test periods, whereas the minimum manufacturer limit was 150 kg/h. However, it is unclear how much this affected the measured 2nd stage total efficiencies since the calculated total efficiencies for the 1st stage compressor were high despite the low calculated mass flow rate.

During normal operation the liquid CO_2 collects in a liquid separator tank. During all tests for compressor behaviour presented in Figure 22 the valves were opened during steady state periodically to test for trapped liquid in the system. There was no noticeable change in the measured conditions upon opening the valves, so it was assumed that the liquid was fully vaporised within the evaporator. One possible explanation for the unexpected results seen in Figure 22 above is therefore that the assumption of complete evaporation in the system was incorrect. This resulted in an unexpected pattern for the compressor behaviour when the valves were opened during the previously assumed steady-state periods. This could possibly be explained because the minimum superheating needed to guarantee complete vaporization in the evaporator depends on the mass flow of CO_2 in the system, yet during all tests the superheat varied from 7-10°C.

In the further tests shown in Figure 23 - Figure 25, the liquid separator valve was only opened after each completed test to ensure steady-state conditions. Compared to Figure 22, the results in Figure 23 - Figure 25 show more of a pattern for 1st stage compressor and 2nd stage compressor behaviour with changing expansion valve outlet pressure. It is difficult to determine a pattern in the data due to the non-ideal testing conditions for the data obtained in Figure 22, and the inconsistent pattern when the data for Figure 23 - Figure 25 was analysed together as seen in Figure 26. One possible reason for the strange results seen in Figure 26 is that some liquid was trapped in the system

between morning and afternoon tests. More work needs to be done to test this theory and to develop a better prediction for the compressor pressure ratios as a function of the expansion valve outlet pressure.

As mentioned in the Model methodology section, an assumption was needed for the model to calculate the refrigerant bulk temperature from the wall temperatures around the evaporator. This assumption is also very important for the mass flow calculation in the 1st stage compressor part of the model since this calculation requires the density of the flow, but density changes as temperature changes. Since the bulk temperature is estimated, and not a measured value, this increases the uncertainty of the mass flow calculated in the model from the 1st stage compressor. Without a mass flow meter or more advanced temperature measurement devices inside the tubes, this error cannot currently be reduced.

As mentioned in the Results section, the effect of compressor speeds on cycle performance was studied. The model was also programmed with the possibility to change the compressor speeds. Calculations based on measurement data indicated that the 1st stage compressor always operated at much higher total efficiency than the 2nd stage compressor. Also, tests on decreasing the 1st stage compressor speed showed significant decrease in cycle COP. Therefore, it was decided to study only decreases in 2nd stage compressor speed to test the rate of improvement in overall cycle COP. As seen in Figure 27, decreasing 2nd stage compressor RPM resulted in much less compressor work and much higher COP. Although the trend was clear in the results, more test data is needed to develop a model that accurately reflects the modifications to compressor performance when compressor speeds are changed. These further tests should also investigate the lower limit for compressor operating speeds since the 2nd stage compressor outlet pressure is reduced with lower compressor speed.

9.2 Gas cooler

Most of the literature studied and referred to in this report focuses on discussions and predictions about the heat transfer coefficient of CO_2. Despite all studies focusing on the CO_2 heat transfer coefficient, the air side heat transfer coefficient is more important to study in an air-to-CO_2 heat exchanger unit. Although measurement data shows the gas cooler in this experimental setup is an efficient heat exchanger and cools the CO_2 to desired temperatures close to the inlet air temperatures, it was found that the air side is what limits the total heat transferred. This is because the calculated heat transfer coefficients of air for the experimental setup were much lower than those for CO_2, causing the air side to become the limiting side for heat transfer despite much more exposed area.

The calculated gas cooler pressure drop in the model was very small, which is in agreement with the measured and predicted pressure drops from literature. However, during testing with the experimental setup, large pressure drops were measured in the cycle between all units. This is believed to originate from the distribution and recombination of the flow between the single larger tubes and the multiple smaller tubes inside the units.

According to the model, the desired CO_2 outlet temperature from the gas cooler was reached about half way through the unit. The exact position this occurred was dependent on the mass flow. In a previous test it was also confirmed that the gas cooler had a greater tubing capacity than what is needed to achieve the desired refrigerant temperature change. In this test, the temperature of the

inlet CO_2 was significantly increased but the gas cooler still cooled down the CO_2 to the same levels as during normal operation. This can be considered during future design of the gas cooler before large scale manufacture to reduce size and costs.

In addition to the modelled gas cooler for the existing experimental setup, theoretical calculations were performed on a single larger tube gas cooler. A single tube gas cooler would, in theory, reduce the amount of pressure drop significantly due to the absence of the distributor which is believed to cause the majority of the pressure drop. The pressure drop is around 2-3 bar at normal operating conditions with the current gas cooler unit, including the distributor device. An example single tube heat exchanger unit was calculated to have around 1 bar pressure drop given the same CO_2 inlet conditions. Assuming the same heat transfer efficiency as for the multi-tube configuration, a single tube gas cooler unit, would, in theory achieve similar CO_2 outlet temperature given the same area. Note here that the heat transferred per unit of area would be lower, since the single tube unit has less tube area and more fin area. However, since the current gas cooler is proven to be over-dimensioned, approximately the same amount of heat would be transferred. Despite good results from theoretical calculations regarding a single tube unit, it needs to be tested and evaluated before further assumptions can be made.

9.3 Evaporator

The mathematical model created based on common evaporator heat transfer correlations does not match very well with the results analysed from tests performed on the experimental setup. The expected heat transfer predicted from the model is much lower than the actual heat transfer measured in experiments and the minimum heat transfer needed to fully vaporize the liquid. In the same way as for the gas cooler, most of the literature studied and referenced regarding CO_2 cycle evaporators puts major focus into the refrigerant heat transfer coefficients. Also similar to the gas cooler, for the evaporator the air side was proven to be the limiting side for heat transfer for the modelled air flows and heat transfer coefficients. This was also confirmed from various tests with the model where the refrigerant mass flow was increased, thereby increasing the capacity of the cycle. Those tests showed that the liquid CO_2 was not fully vaporized because the air could not provide enough heat. To be able to run the cycle at higher capacity, more air flow must be provided or a design change must take place to increase the air heat transfer coefficient.

Similarly to the gas cooler, the pressure drop calculated inside the evaporator is very small. However, the total pressure drop over the unit when including the distribution and recombination processes becomes relatively large due to the complications in the distribution device. Figure 21 presented in the Results section shows that the distribution sometimes varies very much between different steady-state measurement periods. Uneven distribution of the flow leads to modelling problems because it is impossible to consistently predict the exact distribution within each tube. Therefore, in the model even distribution is assumed which leads to lower pressure drop prediction than actually occurs due to different mass flows and quality in the smaller tubes.

One error source for the initial evaporator model is the heat transfer correlation selected. This correlation was developed by Hwang et al. (1997) from the results of Bredesen et al. (1997), and was able to predict 86% of the authors' measurement data within ±20% (Thome J.R., 2005). This error is expected since, as discussed in the Literature review section, Mastrullo et al. (2010) compared common correlations used for predicting CO_2 heat transfer within an evaporator unit and found that

all the studied correlations resulted in large prediction error when used for larger data sets than the original data set used to develop the correlations.

The Hwang et al. (1997) correlation was initially used in the model due to the inability to use many of the other common correlations. Most of the correlations compared by Mastrullo et al. (2010) require a known heat flux in order to calculate the two-phase heat transfer coefficient. It is not feasible to use these equations for the purposes of this report as the model is required to calculate the heat transfer coefficient and then the heat flux to determine the total heat transfer. Also, the heat flux is not constant in the experimental system discussed in this report. Additionally, many of the correlations are developed for other refrigerants or general fluids, further increasing the uncertainty in the predicted values for CO_2 heat transfer for a given heat flux.

According to the model, when the CO_2 reaches a fully evaporated state in the evaporator it gets very rapidly superheated to temperatures close to the air inlet temperature. This is due to a combination of the fact that the heat exchanger is quite efficient (similar to the gas cooler), and that the temperature changes very rapidly with only small changes in enthalpy. From a standard pressure-enthalpy property diagram for CO_2 it can be seen that the space between the temperature lines is very small and small enthalpy changes can change the temperature significantly at a given pressure. Due to this, the real system and the model are very sensitive to small changes in expansion valve outlet pressure. Due to this sensitivity and the errors associated with the assumptions needed to create the model, the superheat predicted from the model is inconsistent. When testing the model for small variations in expansion valve outlet pressure, most pressure settings give a model result for the superheat around 10°C. However, there is a point where a small change in the expansion valve outlet pressure from one test to the next results in a sudden drop in superheat from around 10°C to almost 0°C. This is due to the sensitivity in modelling the expansion valve pressure and the nature of the enthalpy and temperature relationship in the region close to the saturation curve in the pressure-enthalpy diagram. This sensitivity of the superheat versus expansion valve outlet pressure level prevents the model from accurately predicting a constant superheat value. Despite this issue, the model is able to predict system performance trends that were observed from the measured data. Examples of trends include the approximate expansion valve outlet pressure level where CO_2 is not fully evaporated in the cycle and variation in system COP with respect to expansion valve outlet pressure and ambient air temperature.

One final point to note is that in a similar way as for the gas cooler, a calculation was made to investigate an option to reduce the pressure drop over the evaporator. The same assumptions were made as for the gas cooler calculations. The investigated single tube evaporator unit showed in theory to require more space than the current evaporator unit by about 20 to 30 % because of the lower heat transfer per unit of area. However, the pressure drop was estimated to be reduced from about 3 to 4 bar to around 2 bar for the single tube unit with the same CO_2 outlet temperature as for the existing configuration. If space is available and the design cost is similar, a single tube design could be a possible solution to parts of the pressure losses in a CO_2 cycle such as the existing configuration. However, for mobile applications space is a limiting factor which favours a multi-tube configuration. It should be noted that no literature was found during the development of this report suggesting or presenting a single tube evaporator design concerning CO_2 cycles. It would therefore be interesting to do further calculations and tests on a single tube unit.

9.4 Air side

Despite all the correlations used to calculate the heat transfer coefficients in this report, it is the air side, as stated several times above, that limits the actual heat transferred per unit of area in all the heat exchanger units in the experimental setup. This makes the air flow and the configuration of the heat exchanger units very important for determining cycle performance. Accurate values of the air flow rate were unavailable due to significantly fluctuating values recorded during measurement attempts. However, the measured air flow rates were in range of the predictions from the fan manufacturer and therefore the manufacturer data was assumed to be accurate.

The model is able to accurately predict the heat transfer in the evaporator compared to measurement data. Although these results are important, it is interesting to note that the calculated efficiency of the fins was very low, suggesting potential error when using the simplifying assumptions for the fin heat transfer. Another important point is the uncertainty in the configuration modelled, which could lead to potential error in prediction of the air side heat transfer coefficient despite the apparent accurate results. The configurations of the heat exchangers are not perfectly modelled since the real configurations are not ideal. A staggered configuration as close as possible to reality was modelled.

The choice of heat transfer correlation for the model is also an important factor when considering the accuracy of the predicted heat transfer. The average Nusselt number for the tube bank was modelled using equation (4) for air in cross flow over tube banks without fins. Heat transfer for the fins was then added using the equations describes in the Fins part of the Model methodology section for convective, non-adiabatic fins. After a further literature search, two additional methods were chosen to determine the total air side heat transfer. For one of these methods, a similar Nusselt number equation for air in cross flow over tube banks was used but the correlation was developed for finned tubes. The second method was to model the air flow between the fins as laminar flow through a circular pipe. However, both of these methods resulted in significantly less heat transfer in the evaporator. Therefore, the original Nu correlation used in equation (4) and the fin heat transfer equations presently previously were therefore used for the final version of the model.

Overall, the accuracy of the air flow and the heat exchanger design were shown to be the most important factors concerning heat transfer in this experimental setup. There is most likely a larger potential for improvement of both capacity and COP by modifying the air side than many other modifications such as compressor efficiency or pressure drop reductions within the heat exchanger units.

When the model is run in steady state, the air flow is kept constant over time. This does not correspond to a real transport situation where the real air flow most likely changes over time due to weather, and time of day. Results should therefore be carefully analysed with respect to superheat temperatures in the evaporator, gas cooler and intermediate cooler CO_2 outlet temperatures. These temperatures are strongly dependent on the air flow and the ambient air temperatures. Small changes in these temperatures can lead to large changes in cycle COP or incomplete vaporization in the evaporator.

9.5 One-stage compression

To aid in model creation, tests were conducted on the existing experimental setup to determine typical operating conditions at steady-state. These tests were primarily conducted for two-stage compression. Although much data exists from earlier tests at SP on the experimental setup, none of this data is for steady-state operation in one-stage compression. Attempts to measure steady-state operation in one-stage compression mode for this report continually failed since the compressor always overheated and the system was unable to fully evaporate the CO_2. The source of these problems is unclear as attempts to stabilize the system by changing the mass in the system or the expansion valve outlet pressure were unsuccessful. Additionally, literature study shows significantly better system performance with two stage compression, and most literature studies found while researching this report focused on cycles with only two-stage compression. For these reasons, this report has also focused on two-stage compression of the experimental setup, though future work is needed to research the real operating results for one-stage compression. Although a basic one-stage model has been created from expectations, future work is needed to improve this modelling process and validate this existing model. Modifications can be made to the model when more accurate measurements are recorded and a more accurate pattern is observed in the data for one-stage compression.

9.6 Additional internal heat exchanger

As mentioned previously, the major purposes of this project were to study the existing system and to create a program in MatLab that would aid in future testing of the existing system rather than investigating COP improvements for the existing system. Since future experiments may investigate the use of additional heat exchangers, a very simplified study of future system improvement possibilities was done.

One typical device used for improving the COP in the system is a flash chamber intercooler. With this device, CO_2 expands into a flash chamber after the gas cooler. The vapour in the flash chamber is used to cool down the vapour exiting the intercooler, and the liquid in the flash chamber continues on to the evaporator device. Due to time limitations, it was outside the scope of this report to investigate the use of a flash chamber intercooler. However, the MatLab program was modified to include an additional very basic internal heat exchanger after discussions with project supervisors about likely future system additions. This extra internal heat exchanger was modelled using the CO_2 flow at the evaporator outlet and the intercooler outlet. Although this part of the model was very basic, the results presented in Table 5 of the Model results section show that this simplified heat exchanger would likely be needed to cool down the CO_2 before the 2^{nd} stage compressor in cases where the ambient air into the intercooler is high (near 300 K).

10 Conclusions

There are many conclusions that can be drawn from this project after many weeks of testing and modelling the CO_2 heat pump system. This section presents the major conclusions of the work.

Firstly, the gas cooler in the experimental setup is over-dimensioned. However, both previous studies and tests performed on the experimental setup show that the outlet temperature of the gas cooler strongly influences the system COP. With this said, the current dimensions should be considered positive even if potential space could be saved, especially for mobile applications. In future work, it could be considered to install and test a single tube gas cooler configuration to analyse heat transfer properties and pressure drop behaviour.

Also, despite many studies performed to suggest different heat transfer correlations for mixed-phase CO_2 flow, the air side was shown to be the limiting side for heat transfer in the evaporator in this experimental setup regardless of the CO_2 heat transfer correlation used. Future work should be focused on solving design issues and maximizing the potential heat transfer from the air side rather than the CO_2 side.

Maldistribution in the distributor before the evaporator causes potential problems concerning heat transfer, pressure drop and evaporation rate of the liquid CO_2. This is particularly important as the inability to accurately predict the flow distribution provides an additional source of error for the model. More work needs to be done to analyse how uneven distribution influences the performance of the cycle and pressure drop behaviour over the unit.

The 2nd stage compressor consumed significantly more power than the 1st stage compressor, up to 100% more power consumed in several tests. The reasons for this are unknown, though it is believed that the compressor was not properly designed for the typical high inlet pressures that occur for the 2nd stage in this experimental setup. Suggested future work is to analyse and test other kinds of compressors that are better designed for the high inlet pressures in the 2nd stage in this experimental setup.

Results from limited tests with 2nd stage compressor speed changes showed that significant (up to 20%) improvement in cycle performance could potentially be achieved by lowering the 2nd stage compressor speed. The speed was changed step by step from 1450 RPM down to 1100 RPM with a few steady state measurement points. Therefore, despite possible cost, space and cycle control issues it should be considered to include a compressor frequency converter in mobile applications.

Theoretical calculations for a general case of a simple internal heat exchanger between the evaporator outlet and the intermediate cooler outlet were also briefly studied for this report. According to the very simplified developed model, it would be possible to implement this for operation at higher ambient temperatures and yet maintain similar cycle performance compared to the current system. At an ambient temperature of 298 K, the model predicts the cycle to operate at about 20% less overall efficiency than for an ambient temperature of 280 K. However, it should be noted that this simulation was very simplified and more work needs to be done to further investigate such a change in design.

11 Future work

In this section, a few suggestions are discussed regarding possible future work and improvements that can be made to both the model and the experimental setup.

A new evaporator design would be interesting to test with the current setup since the current evaporator has been shown to perform relatively poor. The authors of this report suggest a new design of the distribution device so that a more even distribution can be achieved. Alternatively, it could be interesting to study a complete new evaporator with fewer inlet tubes after the distributor device to get a better understanding of how the distribution will occur.

More research and work regarding the compressors needs to be done. As mentioned in the discussion section, the low performance of the 2^{nd} stage compressor can depend on many different factors. The authors of this report suggest further tests with a reduction of the 2^{nd} stage compressor speed to see where the limit occurs regarding increased cycle COP performance. Additionally, further investigation regarding why the 2^{nd} stage compressor performs poor at nominal speed needs to be done.

Since the air side is the limiting side regarding the total heat transferred in all units, further tests are recommended to verify the air side assumptions made in this report. Also, as the current model indicates, the system is not able to run without the 2^{nd} stage compressor overheating when high ambient temperatures are present. Therefore it is recommended to install an internal heat exchanger to further increase and test the capacity of the heat pump cycle.

As a final recommendation, the authors would like to suggest a possible future implementation of an ejector-expansion device. This would probably remove the need of a new distributor since only liquid CO_2 then would enter the evaporator. This is not discussed in detail in the report but the authors believe that this design could be beneficial due to the current problems with the flow distribution into the evaporator.

12 Bibliography

Montreal Protocol. (2000). Retrieved 04 10, 2012, from United Nations Environment Programme: Ozone Secretariat: http://ozone.unep.org/new_site/en/Treaties/treaty_text.php?treatyID=2

Ahmad, M. e. (2009). General characteristics of two-phase flow distribution in a compact heat exchanger. *International Journal of Heat and Mass Transfer, Vol 52, Issues 1–2*, 442–450.

B. T. Austin, K. S. (2011). Transcritical carbon dioxide heat pump systems: A review. *Renewable and Sustainable Energy Reviews 15*, 4013– 4029.

Bredesen, A. e. (1997). Heat transfer and pressure drop for in-tube evaporation of CO2. *Proceedings of the International Conference on Heat Transfer Issues in Natural Refrigerants* (pp. 1-15). University of Maryland.

Brix, W. e. (2009). Modelling refrigerant distribution in microchannel evaporators. *International Journal of Refrigeration, Volume 32, Issue 7*, 1736–1743.

Chaobin Dang, E. H. (2004). In-tube cooling heat transfer of supercritical carbon dioxide. Part 1. Experimental measurement. . *International Journal of Refrigeration 27* , 736–747.

Cho, E. e. (2000). A study on the characteristics of evaporative heat transfer for carbon dioxide in a horizontal tube. *Proceedings of the KSME Spring Annual Meeting*, (pp. 104–107).

F.P. Incropera et. al. (2007). *Fundamentals of Heat and Mass Transfer, 6th ed.* John Wiley & Sons.

Grimison, E. D. (1937). Correlation and Utilization of New Data on Flow Resistance and Heat Transfer for Cross Flow of Gases Over Tube Banks. *Trans. ASME 59*, pp. 583-594.

Høgaard, H. e. (1997). Heat transfer coefficient for boiling carbon dioxide. *Proceedings of the International R&D on Heat Pump, Air Conditioning and Refrigeration Systems*, (pp. 113–122). Gatlinburg, TN, USA.

Hwang Y., K. B. (1997). Boiling heat transfer correlation for carbon dioxide. *IIR Conference : Heat Transfer Issues in Natural Refrigerants.* University of Maryland, USA.

J. Pettersen et al. (1998). Development of compact heat exchangers for CO2 air-conditioning systems. *International Journal of Refrigeration Vol. 2, No. 3*, 180-193.

Jardeby, Å. N. (2012). Accordance between a mathematical simulation model and test results from a CO2 heat pump test rig. *10th IIR Gustav Lorentzen Conference on Natural Refrigerants, Delft, The Netherlands*.

Kim, M. e. (2004). Fundamental process and system design issues in CO2 vapor compression systems. *Progress in Energy and Combustion Science 30*, 119-174.

Kim, M. P. (2004). Fundamental process and system design issues in CO2 vapor compression systems. *Progress in Energy and Combustion Science 30*, 119-174.

Lemmon, E. H. (2010). NIST Standard Reference Database 23: Reference Fluid Thermodynamic and Transport Properties-REFPROP, Version 9.0, National Institute of Standards and Technology, Standard Reference Data Program. Gaithersburg.

Marchitto, A. e. (2008). Experiments on two-phase flow distribution inside parallel channels of compact heat exchangers . *International Journal of Multiphase Flow, Vol 34, Issue 2*, 128–144.

Mastrullo et. al. (2010). Carbon dioxide heat transfer coefficients and pressure drops during flow boiling: Assessment of predictive methods. *International Journal of Refrigeration. Volume 33, Issue 6*, 1068–1085.

Nekså, P. (2002). CO2 heat pump systems. *International Journal of Refrigeration 25*, 421-427.

Nekså, P. e. (2010). CO2 - A Refrigerant From The Past With Prospects Of Being One Of The Main Refrigerants In The Future. *9th IIR Gustav Lorentzen Conference 2010 - natural refrigerants – real alternatives.* Sydney.

Ortiz, T. e. (2003). *Evaluation of the performance potential of CO2 as a refrigerant in air-to-air conditioners and heat pumps: system modeling and analysis.* ARTI Final Report ARTI-21CR/610-10030-01.

Park, C. e. (2005). Flow boiling heat transfer of CO2 at low temperatures in a horizontal smooth tube. *Journal of Heat Transfer Vol. 127*, 1305–1312.

Park, C. H. (2007). CO2 and R410A flow boiling heat transfer, pressure drop, and flow pattern at low temperatures in a horizontal smooth tube. *International Journal of Refrigeration 30*, 166-178.

Pearson, A. (2005). Carbon dioxide—new uses for an old refrigerant. *International Journal of Refrigeration 28*, 1140–1148.

Pettersen, J. (1999). Comparison of explosion energies in residential air-conditioning systems based on HCFC-22 and CO2 . *Proceedings of the 20th International Congress of Refrigeration (IIR).* Sydney.

S. H. Yoon et. al. (2003). Heat transfer and pressure drop characteristics during the in-tube cooling process of carbon dioxide in the supercritical region. *International Journal of Refrigeration 26*, 857–864.

S.H. Yoon et. al. (2004). Characteristics of evaporative heat transfer and pressure drop of carbon dioxide and correlation development. *International Journal of Refrigeration 27*, 111–119.

Sarkar, J. (2006). *PhD Thesis: Transcritical carbon dioxde heat pumps for simultaneous cooling and heating.* Kharagpur, India.: IIT.

Sarkar, J. (2010). Review on Cycle Modifications of Transcritical CO2 Refrigeration and Heat Pump Systems. *Journal of Advanced Research in Mechanical Engineering, Vol. 1*, 22–29.

Son, C. P. (2006). An experimental study on heat transfer and pressure drop characteristics of carbon dioxide during gas cooling process in a horizontal tube. *International Journal of Refrigeration 29, Issue 4* , 539–546.

Stera, A. (1992). Ammonia refrigerating plant on reefer ships. Introduction to ammonia as a marine refrigerant. . *Lloyd's Register Technical Seminar.* London.

Thome J.R., R. G. (2005). State-of-the-art of two-phase flow and flow boiling heat transfer and pressure drop of CO2 in macro- and micro-channels. *International Journal of Refrigeration Volume 28, Issue 8*, 1149-1168.

Vist, S. (2004). Two-Phase Refrigerant Distribution in Round Tube Manifolds. *ASHRAE Transactions, Vol. 110*, 307-317.

Vist, S. P. (2002). *Two-phase flow distribution in compact heat exchanger manifolds.* Grenoble: Compact Heat Exchanger Symposium: A Festschrift on the 60th birthday of Ramesh K. Shah.

Vist, S. P. (2003). *Two-phase CO2 distribution in a compact heat exchanger manifold.* Victoria Falls, Zambia: 2nd International Conference on Heat Transfer, Fluid Mechanics and Thermodynamics.

Webb, R. a. (2005). Two-Phase Flow Distribution to Tubes of Parallel Flow Air-Cooled Heat Exchangers. *Heat Transfer Engineering Vol 26, Issue 4*.

Yun et. al. (2003). Boiling heat transfer and dryout phenomenon of CO2 in a horizontal smooth tube. *International Journal of Heat and Mass Transfer 46*, 2353–2361.

Zukauskas, A. (1972). Heat Transfer from Tubes in Cross Flow. In J. E. J.P. Hartnett and T.F. Irvine, *Advances in Heat Transfer, Vol. 8.* New York: Academic Press.

13 Nomenclature

A	area	[m^2]
A_c	cross sectional area	[m^2]
A_f	surface area	[m^2]
C	constant for airflow in a tube bank	[---]
c_p	specific heat under constant pressure	[J/(kg.K)]
D	diameter	[m]
f	friction factor	[---]
G	mass velocity	[kg/(m^2.s)]
g	gravity	[N/kg]
H	enthalpy	[J/kg]
h	convective heat transfer coefficient	[W/ m^2.K)]
k	thermal conductivity	[W/(m.K)]
L	length	[m]
L_c	equivalent length	[m]
M	coefficient for fin heat transfer	[W]
$\dot{m}$	mass flow rate	[kg/s]
m	constant for airflow in a tube bank	[---]
m	coefficient for fin heat transfer	[1/m]
N	compressor speed	[rpm]
N	number of tube rows	[---]
P	pressure	[bar]
Pr	Prandtl number	[---]
Re	Reynolds number	[---]
Nu	Nusselt number	[---]
T	temperature	[°C, K]
$\dot{Q}$	heat transfer rate	[W]
$R_{t,b}$	thermal resistance at fin base	[K/W]
$R_{t,f}$	thermal resistance of the fin	[K/W]
S	pitch	[m]
S	coefficient	[---]
t	fin thickness	[m]
V_s	swept volume of compressor	[m^3]
V	velocity	[m/s]
$\dot{W}$	electrical power	[W]
w	fin width	[m^2]
X_{tt}	Martinelli number	[---]
x	quality	[%]

Greek

η	efficiency	[%]
ρ	density	[kg/m^3]
ε	efficiency, effectiveness	[---]
Δ	variation	[---]
μ	dynamic viscosity of fluid	[Pa/ s]
σ	surface tension	[N/m]
θ_b	temperature difference	[K]
Φ	two-phase multiplier	[---]
β	compressor pressure ratio	[---]

Subscripts

air	air
b	bulk, base of fin
bc	convection
D	diagonal
el	electric
fin	fin
g	gas
I	inside
in	inlet, in
is	isentropic
L	longitudinal
l	liquid
lo	liquid only
lv	vapor minus liquid property
mech,el	mechanical and electrical
max	maximum
meas	measured (electrical)
min	minimum
nb	nucleate boiling
o	outside
out	outlet, out
pass	tube pass in heat exchanger units
pc	pseudo-critical
r	refrigerant
sat	saturation
seg	segment
T	transverse
tot	total
tp	two-phase
v	vapour, volumetric
vo	vapour only
w	wall
∞	fin tip
1^{st}	1^{st} stage compressor
2^{nd}	2^{nd} stage compressor

14 Appendix

14.1 Model process

A simplified version of the final modelling process for two stage compression is provided here to aid the reader in understanding the work described in the sections above.

1. Request model inputs such as compressor speeds, outside air temperature, expansion valve outlet pressure and desired graphical output mode (Temperature-enthalpy, or Pressure-enthalpy curves).
2. Calculate mass flow of CO_2 from the 1st stage compressor. Use this to determine the inlet and outlet conditions of the compressor, as well as compressor work.
3. Run code for intermediate cooler heat exchanger to determine 2nd stage compressor inlet conditions of the CO_2.
4. Determine the outlet conditions of 2nd stage compressor, as well as compressor work. Note: the 2nd stage compressor pressure ratio is determined from the 1st stage pressure ratio and the expansion valve outlet pressure based upon measurement data.
5. Run code for gas cooler heat exchanger to determine expansion valve inlet conditions for the CO_2.
6. Assume isenthalpic expansion process to calculate the evaporator inlet quality, temperature, and pressure
7. Use the expected air heat transfer in the evaporator, enthalpy of vaporization, refrigerant mass flow, and the calculated values from step 6 to predict the CO_2 properties at the evaporator outlet
8. Update the refrigerant mass flow prediction from the calculated evaporator outlet conditions from step 7
9. Iterate the program using the new mass flow prediction until the difference in mass flow calculations from each iteration is sufficiently small
10. Output results

14.2 Data examples

Due to security reasons and space limitations for each page, an example of the measurement data logs for one test day is not included in this report. To provide a basic idea of the measurement data analysis, some raw data has been included here. The figures are included as examples of the measurement data that was used to calculate steady-state cycle values and later used to aid in the model creation.

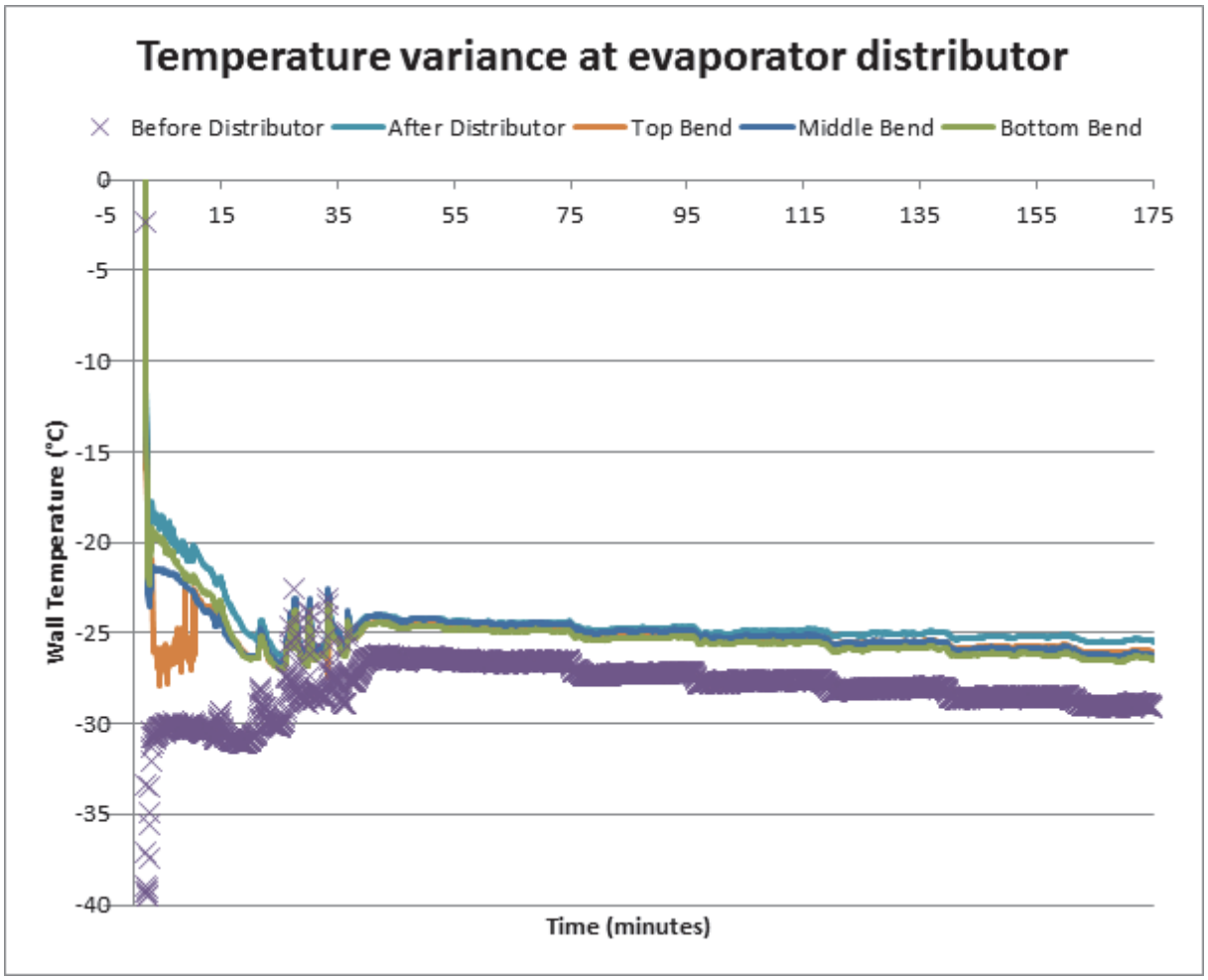

Figure 30. Example from 27-04-2012 showing relatively even CO_2 distribution after the evaporator.

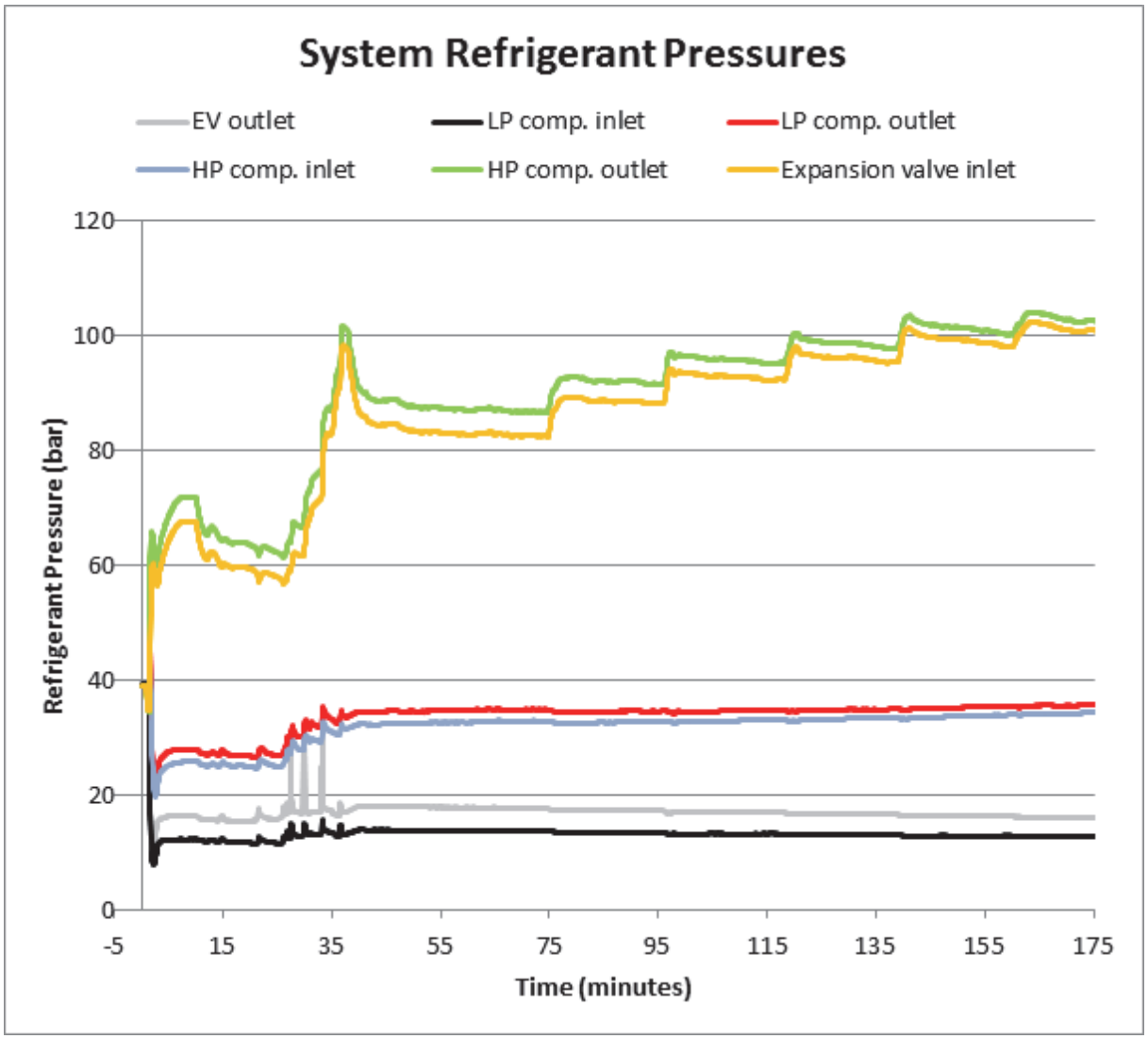

Figure 31. Example from 27-04-2012 showing relatively even CO_2 distribution after the evaporator

Table 6. Modified example of raw measurement data

Temperature indicators		
GT1:1	°C	-15.242
GT1:2	°C	-11.7793
GT1:3	°C	87.38904
GT2:2	°C	11.87549
GT2:3	°C	110.3778
GT2:4	°C	13.15949
T CO2 EV pre distributor	°C	-26.4646
T CO2 in EV	°C	-24.3813
T CO2 EV pipe 1	°C	-24.7006
T CO2 EV mid pipe	°C	-24.3704
T CO2 EV pipe 9	°C	-24.7688
T CO2 out EV	°C	-16.3161
T air in EV (average)	°C	-14.7959
T air out EV (average)	°C	-20.571
T superheat EV	°C	11.1431
T air in GC	°C	7.44849
T air out GC	°C	20.86197
Pressure indicators		
GP1:1	Bar	17.78604
GP1:2	Bar	13.68582
GP1:3	Bar	34.54512
GP2:1	Bar	82.30879
GP2:2	Bar	82.5127
GP2:3	Bar	86.78839
GP2:4	Bar	32.51823
Flow measurements		
Flow GC (average)	m^3/h	0.914945
Flow EV (average)	m^3/h	0.897751
Energy calculations		
Energy GC (average)	W	13496.49
Energy EV (average)	W	-5494.61
Compressor HP	W	3599.474
Compressor LP	W	2393.806
Fan GC	W	568.4183
Fan EV	W	614.0827
COP		0.916795

Table 6 above show the different measurements and calculations done while running the experimental setup. The table above is a “snapshot” of the system and is an example of what the indicators could show at a certain point in time. The indicators named GT1:1-3 and GT2:2-4 are temperature measurements for the CO_2 before and after the major components (the measurement points are illustrated in Figure 2). Similarly, GP1:1-3 and GP2:1-4 are pressure indicators for the CO_2 before and after the major components in the experimental setup. At the inlet of the evaporator, many temperature indicators were installed as previously described. The air temperature at the different inlets and outlets as well as the CO_2 superheat temperature after the evaporator was also measured.

Power and energy consumption from the different units were also measured. The system COP is based on the energy output from the evaporator divided by the energy input into the system.

The abbreviations GC, EV, LP and HP stand for gas cooler, evaporator, low pressure and high pressure respectively. COP stand for coefficient of performance.

CHALMERS UNIVERSITY OF TECHNOLOGY
SE 412 96 Göteborg, Sweden
Phone: + 46 - (0)31 772 10 00
Web: www.chalmers.se